INSTITUTE FOR FUSION STUDIES

DE-FG03-96ER-54346-750 IFSR #750

High-Mode-Number Ballooning Modes in a Heliotron/Torsatron System: II. Stability

N. NAKAJIMA[a)]
Institute for Fusion Studies
The University of Texas at Austin
Austin, Texas 78712 USA

[a)] Permanent address: National Institute for Fusion Science, Nagoya 464-01, Japan

May 1996

THE UNIVERSITY OF TEXAS

AUSTIN

DISCLAIMER

High-mode-number ballooning modes in a heliotron/torsatron system: II. Stability

N. Nakajima[a)]

Institute for Fusion Studies, The University of Texas at Austin

Austin, Texas 78712 USA

Abstract

As described in the companion paper [N. Nakajima, Phys. Plasmas (1996)], in heliotron/torsatron systems that have a large Shafranov shift, the local magnetic shear is found to have no stabilizing effect on high-mode-number ballooning modes at the outer side of the torus, even in the region where the global shear is stellarator-like in nature. The disappearance of this stabilization, in combination with the compression of the flux surfaces at the outer side of the torus, leads at relatively low values of the plasma pressure to significant modifications of the stabilizing effect due to magnetic field-line bending on high-mode-number ballooning modes—specifically, that the field-line bending stabilization can be remarkably suppressed or enhanced. In an equilibrium that is slightly Mercier-unstable or completely Mercier-stable due to peaked pressure profiles, such as those used in standard stability calculations or observed in experiments on the Compact Helical System [S. Okamura,*et al.* Nucl. Fusion **35**, 283 (1995)], high-mode-number ballooning modes are destabilized due to these modified stability effects, with their eigenfunctions highly localized along the field line. Highly localized mode structures such as these cause the ballooning mode eigenvalues ω^2 to have a strong field line dependence (i.e., α-variation) through the strong dependence of the local magnetic curvature, such that the level surfaces of $\omega^2(\psi, \theta_k, \alpha)$ (≤ 0) become spheroids

[a)]Permanent address: National Institute for Fusion Science, Nagoya 464-01, Japan

in (ψ, θ_k, α) space, where ψ labels flux surfaces and θ_k is the radial wavenumber. Because the spheroidal level surfaces for unstable eigenvalues are surrounded by level surfaces for stable eigenvalues of high-mode-number toroidal Alfvén eigenmodes, those high-mode-number ballooning modes never lead to low-mode-number modes. In configuration space, these high-mode-number modes are localized in a single toroidal pitch of the helical coils, and hence they may experience substantial stabilization due to finite Larmor radius effects.

PACS: 52.35.Py, 52.55.Hc

I. INTRODUCTION

The companion paper[1] examined the characteristics of the local magnetic shear in relation to the properties of equilibrium quantities in an $L = 2/M = 10$ heliotron/torsatron system like the Large Helical Device (LHD)[2]. Here, L and M are the polarity and toroidal pitch number of the helical coils, respectively. In Ref. 1 it was shown that the stabilizing effects due to the local magnetic shear $\hat{s}$ can disappear on the outer side of the torus, even in the region of stellarator-like strong global magnetic shear with $s \equiv 2\frac{d\ln\iota}{d\ln\psi} > 0$, where ι is the global rotational transform and ψ is the flux surface label, with the latter being related to the toroidal flux Φ_T inside the flux surface ψ through $\Phi_T = 2\pi\psi$. Also, it is pointed out in Ref. 1 that the vanishing of the local magnetic shear is a universal feature, at least in $L = 2$ heliotron/torsatron systems with a large Shafranov shift.

In the present paper, we combine these properties of the stabilizing effects due to the local magnetic shear with those of the destabilizing effects caused by the local magnetic curvature and analyze the stability of high-mode-number ballooning modes in an $L = 2/M = 10$ heliotron/torsatron system. We also clarify the relation of these modes to low-mode-number modes.

The spectrum of ballooning modes in general toroidal systems has been investigated in Ref. 3. In that work, a model tokamak with toroidal field ripple was used as an example in order to study the affects of symmetry breaking on the ballooning spectrum. The level surfaces for the eigenvalues were categorized in (ψ, θ_k, α) space, where α labels the magnetic field lines on the flux surface ψ, and θ_k is the radial wavenumber. The eigenvalues whose level surfaces are topologically cylindrical were intensively examined, because those surfaces are the ones that continuously connect to the level surfaces for an axisymmetric tokamak when the toroidal ripple is reduced.

Recently, an examination similar to that in Ref. 3 was carried out for high-mode-number ballooning modes in an LHD equilibrium with a broad pressure profile, thus strongly Mercier-unstable.[4] In that work, to compare the results from the high-mode-number ballooning analysis with those from the low-mode-number ballooning analysis, the high-mode-number ballooning equation was modified so as to give the same kinetic energy norm as in the low-mode-number equation. With this modification, the results from both analyses were consistent; however, it was not clear how the kinetic energy norm affected the level surfaces for the eigenvalues so obtained. Modifying the kinetic energy norm might induce a topological change in the level surfaces for the eigenvalues, e.g., from cylindrical-type level surfaces to spheroidal-type level surfaces or vice versa in (ψ, θ_k, α) space.

In this paper, we will investigate the stability properties of high-mode-number ballooning modes, both in strongly Mercier-unstable equilibria and in slightly Mercier-unstable or completely Mercier-stable equilibria, for an $L = 2/M = 10$ heliotron/torsatron system with a large Shafranov shift, with the use of the exact incompressible three-dimensional high-mode-number ballooning mode equation.[5] The same vacuum magnetic configuration as in Ref. 1 is used. The strongly Mercier-unstable equilibria correspond to broad pressure profiles, and the slightly Mercier-unstable or completely Mercier-stable equilibria[6] correspond to peaked pressure profiles. Depending on whether the Mercier criterion can be easily violated, the stability properties of the high-mode-number ballooning modes change, and this change is reflected in the topological structure of the level surfaces for the eigenvalues. This feature is important when the relationship between high- and low-mode-number modes and also what toroidal mode numbers should be expected is considered. In Sec. II, the global characteristics of the equilibria with either broad or peaked pressure profiles are indicated. The local characteristics of these equilibria are described in Sec. III. In Sec. IV the stability properties of high-mode-number ballooning modes are examined in terms of the global and local equilibrium characteristics. The relationship between high- and low-mode-number bal-

looning modes and the influence of kinetic effects, such as finite Larmor radius (FLR), on the high-mode-number modes are also addressed. Section V contains discussion.

II. GLOBAL EQUILIBRIUM CHARACTERISTICS

For the vacuum configuration, we will use the planar-axis $L = 2/M = 10$ heliotron/torsatron configuration of Ref. 1. Currentless equilibria with finite-β, where β is the ratio of the plasma kinetic pressure to the magnetic field pressure, will be calculated with the use of the VMEC code[7] for fixed boundary conditions, with the boundary determined as the outermost flux surface of the vacuum field. Two types of pressure profiles will be used in order to examine the relationship of Mercier stability to that of high-mode-number ballooning modes: a peaked profile, given by

$$P(\psi_N) = P_0(1 - \psi_N)^2, \tag{1}$$

and a broad profile, given by

$$P(\psi_N) = P_0(1 - \psi_N^2)^2. \tag{2}$$

Here $\psi_N = \frac{\psi}{\psi_{\rm edge}}$ is the normalized toroidal flux, with $r_N = \sqrt{\psi_N}$ the normalized minor radius. Note that the peaked pressure profile given in Eq. (1) is the profile that is normally used in stability calculations for the LHD,[6] and that peaked pressure profiles similar to that given in Eq. (1) are observed in ordinary experiments in Compact Helical System (CHS).[8]

Figure 1 shows the global rotational transform ι, the global magnetic shear $s \equiv \frac{2\psi}{\iota}\frac{d\iota}{d\psi}$, the index of the averaged magnetic well quantity V'' that measures the average magnetic well (here a prime indicates the derivative: $' \equiv \frac{d}{d\Phi_T}$), and the Mercier criterion parameter D_M as functions of the normalized toroidal flux. The upper set of graphs exhibit these quantities for the peaked pressure profile of Eq. (1), and the lower set for the broad pressure profile of Eq. (2). The three curves in each graph correspond to different central β values: $\beta_0 = 0$ (dotted curve), 4% (dot-dashed curve), and 8% (solid curve). For the vacuum configuration

considered here, the Shafranov shift is quite large, i.e., there is a substantial Pfirsch-Schlüter current. Consequently, the global rotational transform ι and the global magnetic shear s become highly deformed as β increases for both types of pressure profiles. In particular, the global rotational transform ι increases near the magnetic axis, but decreases near the periphery. Because a region of tokamak-like global magnetic shear appears near the magnetic axis and the stellarator-like magnetic shear is increased near the periphery, a shearless region occurs between them, as can be seen in the graphs in Fig. 1 for the global magnetic shear. As β increases, the global magnetic shear becomes very strong in the stellarator-like region near the plasma periphery. Note, from Fig. 1, that all the curves for the global rotational transform ι cross each other at the same flux surface, for both peaked and broad pressure profiles; this feature was analytically explained in Eq. (79) of Ref. 1. The occurrence of the tokamak-like region of global magnetic shear near the magnetic axis is more evident for the peaked pressure profile than for the broad pressure profile because the corresponding Shafranov shift is larger, as will be later shown in Figs. 2 and 3. For the same reason, the average magnetic well for the peaked pressure profile ($V'' < 0$) is deeper than that for the broad pressure profile, as shown in Fig. 1.

The behavior of the Mercier criterion parameter D_M as shown in Fig. 1 can be understood if we rewrite its expression in the following way:

$$D_M = \frac{(\iota')^2}{4} - P'V' \left\{ \left\langle \frac{B^2}{|\nabla\Phi_T|^2} \right\rangle \left[-V'' + \frac{2\pi I \iota'}{\langle B^2 \rangle} \right] + \iota' \left\langle \frac{(\mathbf{J}\cdot\mathbf{B})_{PSN}}{|\nabla\Phi_T|^2} \right\rangle \right\}$$
$$- (P'V')^2 \left\{ \left\langle \frac{(\mathbf{J}\cdot\mathbf{B})^2_{PSN}}{|\nabla\Phi_T|^2 B^2} \right\rangle \left\langle \frac{B^2}{|\nabla\Phi_T|^2} \right\rangle - \left\langle \frac{(\mathbf{J}\cdot\mathbf{B})_{PSN}}{|\nabla\Phi_T|^2} \right\rangle^2 + \left\langle \frac{1}{B^2} \right\rangle \right\}, \qquad (3)$$

with $\langle f \rangle \equiv \frac{d}{dv} \int f d\tau$. Also, $2\pi I$ is the net toroidal current inside the flux surface, and the Pfirsch-Schlüter current divided by P' is given by

$$(\mathbf{J}\cdot\mathbf{B})_{PSN} = -\mathbf{B}\times\nabla\Phi_T\cdot\nabla\tilde{\beta}_N, \quad \mathbf{B}\cdot\nabla\tilde{\beta}_N = 1 - \frac{B^2}{\langle B^2 \rangle}. \qquad (4)$$

The expression in Eq. (3) was obtained, with some manipulations, from Ref. 9. Mercier stability corresponds to satisfying the condition $D_M > 0$. The first term on the right-hand side of Eq. (3) represents shear stabilization. The last term is destabilizing, due to the Pfirsch-Schlüter current (geodesic curvature) and the diamagnetic current. Only the second term can change sign, depending on the average magnetic well quantity V'' and the global magnetic shear ι' for a currentless ($I = 0$) equilibria. Note that in the $L = 2/M = 10$ heliotron/torsatron system being considered here, the inequality $\left\langle \frac{(\mathbf{J}\cdot\mathbf{B})_{PSN}}{|\nabla\Phi_T|^2} \right\rangle 0$ holds. With the use of the relationship $V' = \frac{2\pi(J+\iota I)}{\langle B^2\rangle}$, we can write Eq. (3) as follows:

$$D_M = \frac{(\iota')^2}{4} - P'V' \left\{ \left\langle \frac{B^2}{|\nabla\Phi_T|^2} \right\rangle V' \frac{\langle B^2\rangle'}{\langle B^2\rangle} + \iota' \left\langle \frac{(\mathbf{J}\cdot\mathbf{B})_{PSN}}{|\nabla\Phi_T|^2} \right\rangle \right\}$$

$$- (P'V')^2 \left\{ \left\langle \frac{(\mathbf{J}\cdot\mathbf{B})^2_{PSN}}{|\nabla\Phi_T|^2 B^2} \right\rangle \left\langle \frac{B^2}{|\nabla\Phi_T|^2} \right\rangle - \left\langle \frac{(\mathbf{J}\cdot\mathbf{B})_{PSN}}{|\nabla\Phi_T|^2} \right\rangle^2 + \left\langle \frac{1}{B^2} \right\rangle + \frac{1}{\langle B^2\rangle} \right\}. \quad (5)$$

Thus, it is clear that having an average magnetic well, i.e., $\langle B^2\rangle'(> 0)$, and having positive global magnetic shear, i.e., $\iota'(> 0)$, are critical for Mercier stability.

For an $L = 2/M = 10$ heliotron/torsatron system with a large Shafranov shift, the dominant contribution to Mercier stabilization near the magnetic axis, where the global magnetic shear is weak, comes from the magnetic well term, i.e., ($V'' < 0$ or $\langle B^2\rangle' > 0$), whereas the dominant contribution to Mercier stabilization near the plasma periphery is the global magnetic shear term, $\frac{(\iota')^2}{4}$, since a magnetic hill, i.e., $V'' > 0$ or $\langle B^2\rangle' < 0$, occurs here. For the peaked pressure profile with its monotonically increasing gradient, these two stabilizing contributions work well together, so that an equilibrium with $\beta_0 = 4\%$ that is slightly Mercier-unstable becomes completely stabilized when β_0 exceeds approximately 7%. This behavior implies the existence of second stability for the Mercier criterion, as shown in Fig. 1 in the upper graph for D_M. In contrast, the broad pressure profile has its steepest gradient in the magnetic hill region where $V'' > 0$ or $\langle B^2\rangle' < 0$. Since this strongly destabilizing effect cannot be overcome by the magnetic shear term, the equilibrium with

the broad pressure profile is quite Mercier unstable, as indicated in the lower graph for D_M in Fig. 1.

III. LOCAL EQUILIBRIUM CHARACTERISTICS

A. Local magnetic shear

For the sake of completeness, the local magnetic shear examined in Ref. 1 is briefly discussed. The Boozer coordinate system[8] uses the radial, poloidal, and toroidal coordinates (ψ, θ, ζ). Equally spaced (ψ, θ) meshes in the Boozer coordinate system, for both the peaked and broad pressure profiles, are shown in Fig. 2 on a horizontally elongated poloidal cross section and in Fig. 3 on the vertically elongated poloidal cross section. The upper graphs in Figs. 2 and 3 are for the peaked pressure profile, and the lower graphs for the broad pressure profile. In both Figs. 2 and 3, the three upper graphs correspond, respectively, to the central beta values of $\beta_0 = 0, 4,$ and 8% (from left to right), and likewise for the lower graphs. The peaked pressure profile leads to a larger Shafranov shift than does the broad pressure profile, as can be seen in Figs. 2 and 3.

Another useful covering space is the field line coordinate system (ψ, η, α), which is related to the Boozer coordinate system (ψ, θ, ζ) as

$$\eta = \theta, \qquad \alpha = \zeta - \frac{1}{\iota}\theta, \tag{6}$$

In Ref. 1 it was described how the local magnetic shear $\hat{s}$ can be expressed in terms of the global magnetic shear s and its oscillatory component $\tilde{s}$, as follows:

$$\hat{s} = s + \tilde{s}, \quad s = \frac{2\psi}{\iota}\frac{d\iota}{d\psi}, \quad \tilde{s} = \frac{\partial}{\partial\eta}\left\{\frac{2\psi(Jg_{\psi\theta} - Ig_{\psi\zeta})}{\sqrt{g}|\nabla\psi|^2}\right\}, \tag{7}$$

Here the various metric components are defined as

$$\sqrt{g} = \frac{J + \iota I}{B^2}, \quad g_{ij} = \partial_i R \partial_j R + R^2 \partial_i\phi\partial_j\phi + \partial_i Z \partial_j Z, \quad i, j = \psi, \theta, \zeta. \tag{8}$$

Also, $2\pi J$ and $2\pi I$ is the poloidal net current outside of the flux surface, $2\pi I$ is the toroidal net current inside the flux surface, and α is the label for the magnetic field lines. Note that $I = 0$ for a currentless equilibria. From Eq. (7), the integrated local magnetic shear along a magnetic field line is given by

$$\int^{\eta} \widehat{s} d\eta = s(\eta - \theta_k) + \frac{2\psi(J g_{\psi\theta} - I g_{\psi\zeta})}{\sqrt{g}|\nabla\psi|^2}, \tag{9}$$

with θ_k the radial wavenumber. The domain of the covering space is $\psi_{\min} < \psi < \psi_{\max}$ and $-\infty < \eta, \alpha < \infty$. In the coordinate system used here, $\theta = 0$ or $\eta = 0$ corresponds to the outer side of the torus. The oscillatory component $\widetilde{s}$ is determined by how much local compression of the poloidal field on the outer side of the torus is needed to maintain toroidal force balance. In the Boozer coordinate system, the magnetic field lines are represented as straight lines, and the toroidal angle ζ is very similar to the geometrical toroidal angle in a planar axis heliotron/torsatron system.[1] Therefore, almost all the information about the local compression of the poloidal field appears in the behavior of the poloidal angle θ, as can be seen in Figs. 2 and 3. Thus, $\widetilde{s}$ has a component proportional to $g_{\psi\theta}$ in Eqs. (7) and (9). Near the magnetic axis, the global magnetic shear s is tokamak-like ($s < 0$) for the peaked pressure profile or very small ($s \sim 0$) for the broad pressure profile; this property can be seen in the upper and lower graphs for s in Fig. 1. Therefore, the local compression of the poloidal field increases radially outward in order to maintain toroidal force balance: $g_{\psi\theta} \sim c \sin\theta$ with $c > 0$, which leads to the situation with $s \lesssim 0$ and $\widetilde{s} > 0$. In contrast, near the plasma periphery, the global rotational transform exceeds unity and the global magnetic shear s is strongly stellarator-like ($s > 0$). The local compression of the poloidal field decreases radially outward, due to the large poloidal field on average: $g_{\psi\theta} \sim c \sin\theta$ with $c < 0$, which leads to the situation with $s > 0$ and $\widetilde{s} < 0$. Figures 2 and 3 show that for both types of cross sections and both types of pressure profiles, as the value of β_0 increases, there appears a *turning surface* (i.e., where $g_{\psi\theta} = 0$), whose location depends on the global

rotational transform ι and the pressure profile.[1]

The reduction of the stabilizing effect of the local magnetic shear is exhibited in Fig. 4(a), where the integrated local shear, $\left[\int^{\eta} \widehat{s} d\eta\right]^2$, for $\theta_k = 0$, is plotted along a field line for the peaked pressure profile equilibrium, with $\beta_0 = 8\%$. For this graph, the field line with $\psi_N = 0.56$ and $\alpha = 0$ was chosen; on a horizontally elongated cross section, this field line passes through the outer midplane of the torus. Note that the position at which $\eta = 0$ corresponds to the outer midplane of the torus. For reference, the average integrated local shear $(s\eta)^2$ is also plotted in Fig. 4(a). The same two quantities are shown in Fig. 5(a), but for the equilibrium with the broad pressure profile, with $\beta_0 = 4\%$; here, the magnetic field line with $\psi_N = 0.39$ and $\alpha = 0$ was chosen. This field line also passes through the outer midplane of the torus on a horizontally elongated cross section. Both the $\psi_N = 0.56$ and the $\psi_N = 0.39$ flux surfaces are located in the region where the global shear is stellarator-like in nature. By comparing Figs. 4(a) and 5(a), we find that as β increases, the stabilizing effect of the local magnetic shear near $\beta = 0$ is significantly reduced.

The monotonically increasing profile of the global rotational transform ι near the periphery of a finite-β plasma basically comes about from the vacuum configuration, as can be seen in Fig. 1. Hence, the vanishing of the (integrated) local magnetic shear at the outer side of the torus does not strongly depend on either the type of pressure profile or the magnetic field line label α as the value of β increases. It follows that the stabilizing effect of the integrated local magnetic shear on high-mode-number ballooning modes is not much influenced by the pressure profile or the magnetic field line label α, except that the critical β value at which the local magnetic shear vanishes does depend on the pressure profile. The reduction (or disappearance) of the stabilizing effect of the local magnetic shear in the region where the global shear is stellarator-like is a universal feature, at least in $L = 2$ heliotron/torsatron systems with a large Shafranov shift, since it is caused by the Shafranov shift (i.e., toroidal force balance) for the stellarator-like global magnetic shear inherent in such systems.

B. Local shape of flux surfaces

At the outer side of the torus, the flux surfaces are locally compressed, because this is where the compression of the poloidal field varies radially. This situation is reflected in the local shape of the flux surfaces at the outer side of the torus, as expressed by $|\nabla\psi|$. As shown in the poloidal cross sections with $\beta_0 = 8\%$ in Figs. 2 and 3, the variation of $|\nabla\psi|$ in the minor radius direction significantly changes across the *turning surface* on the outer side of the torus. At the outer side of the torus, adjacent flux surfaces become progressively nearer to each other in radius as the *turning surface* is approached. In other words, the flux surfaces become more and more compressed. Once the *turning surface* is crossed, however, the flux surfaces become less compressed radially. The local compression of the flux surfaces at the outer side of the torus causes the flux surfaces to be locally uncompressed at the inner side of the torus due to toroidal flux conservation. Thus, the change of the local shape of a flux surface $|\nabla\psi|$ along a field line is quite noticeable; this is shown in Figs. 4(b) and 5(b) where the variation of the quantity $\frac{|\nabla\psi|^2}{2\psi B_0}$ is plotted along the same field lines as in the top graphs. The dashed line in each of these graphs, shown for reference, is the approximate value of $\frac{|\nabla\psi|^2}{2\psi B_0} = 1$ for a low-β tokamak with concentric circular flux surfaces. As β increases, $|\nabla\psi|$ is enhanced on the outer side of the torus, but reduced on the inner side. The variation of $|\nabla\psi|$ along a field line becomes most significant in the vicinity of the *turning surface*, where the interval between successive flux surfaces is smallest. Since it is caused by toroidal force balance (i.e., the Shafranov shift), the local compression or decompression of the flux surfaces becomes most noticeable as the value of β increases; however, it is independent of α, the magnetic field line label. Both of these features can be observed in Figs. 2 and 3 if one examines the variation with β_0 and with the poloidal cross section.

The variation of the local shape of the flux surfaces $|\nabla\psi|$ plays an important role in the stabilization of high-mode-number ballooning modes for equilibria with large Shafranov

shifts. The reason for this can be seen from the expression for the perpendicular wavenumber $|\mathrm{k}_\perp|$,

$$|\mathrm{k}_\perp|^2 = \frac{|\nabla\psi|^2}{2\psi B_0}\left[\left(\frac{2\psi B}{|\nabla\psi|^2}\right)^2 + \left[\int^\eta \hat{s}d\eta\right]^2\right], \tag{10}$$

where the secular stabilizing term, which is the dominant term in $|\mathrm{k}_\perp|^2$, has the following form:

$$\frac{|\nabla\psi|^2}{2\psi B_0}\left[\int^\eta \hat{s}d\eta\right]^2 = \frac{1}{2\psi B_0}\left[s(\eta-\theta_k)|\nabla\psi| + \frac{2\psi(Jg_{\psi\theta} - Ig_{\psi\zeta})}{\sqrt{g}|\nabla\psi|}\right]^2. \tag{11}$$

The secular stabilizing term $s(\eta-\theta_k)|\nabla\psi|$ is amplified through $|\nabla\psi|$ each time the field line transits the outer side of the torus, near $\eta = \pm 2p\pi$ with p an integer, leading to an enhancement of its stabilizing effect. On the other hand, each time the field line transits the inner side of the torus, near $\eta = \pm(2p+1)\pi$, the secular stabilizing term is diminished through $|\nabla\psi|$, leading to the reduction of its stabilizing effect. The characteristics of the local shape of the flux surfaces as expressed by $|\nabla\psi|$ are universal, at least for $L = 2$ heliotron/torsatron systems.

In Figs. 4(c) and 5(c), the square of the wavenumber $|\mathrm{k}_\perp|^2$ is plotted along the same field line as that for Figs. 4(a) and 5(a), respectively. These graphs show that the field line bending stabilization effect on high-mode-number ballooning modes is strongly modified as β is increased in an $L = 2$ heliotron/torsatron system with a large Shafranov shift. Within one poloidal period along the field line ($|\eta| < \pi$), this stabilizing effect is significantly suppressed, both because the local shear associated with the poloidal field which is compressed at the outer side of the torus vanishes (Fig. 4(a)) and because the flux surfaces on the inner side of the torus are decompressed (Fig. 4(b)). On the other hand, this stabilizing effect is significantly enhanced farther out along the field line ($|\eta| \sim 2\pi$) due to the local compression of the flux surfaces at the outer side of the torus (Fig. 4(b)). This sort of modification is universal in $L = 2$ heliotron/torsatron systems with a large Shafranov shift and is almost independent of both the magnetic field line label and the pressure profile, except for the β

value at which the modification becomes significant.

C. Local magnetic curvature

The local magnetic curvature in heliotron/torsatron systems consists of two components. One component is due to toroidicity, just as in a tokamak plasma. This mainly comes from the vacuum toroidal field and hence has no dependence on α. The other component is due to helicity (i.e., of the helical coils), which mainly arises from the saddle-like profile for the magnetic field strength, reflecting that in a straight helix. On every poloidal cross section, the outside of the torus corresponds to locally "bad" magnetic curvature, and the inside to "good" curvature, in terms of the toroidicity contribution. In terms of the helicity contribution, however, the regions between the helical coils correspond to the locally bad magnetic curvature in each poloidal cross section, and the regions under the helical coils to locally good curvature. The variation of the magnetic field strength due to the helicity is comparable with that due to the toroidicity. Therefore, the local magnetic curvature is worst at the outer side of the torus in a horizontally elongated poloidal cross section (cf. Fig. 2). At the outer side of the torus in a vertically elongated poloidal cross section (cf. Fig. 3), the locally bad magnetic curvature due to the toroidicity is canceled by the locally good magnetic curvature due to the helicity. Thus, the local magnetic curvature at the outer side of the torus strongly depends on α, the label of the magnetic field line in the covering space (ψ, η, α). This situation is completely different from that in a tokamak plasma. In a tokamak plasma, the local magnetic curvature is independent of the field line label α because of the toroidal symmetry.

The dependence of the local magnetic curvature on the pressure profile is not clear, because the effect of the pressure profile on the local magnetic curvature mainly enters through the shape of the flux surface, as can be seen from the expression for the magnetic

curvature:

$$\boldsymbol{\kappa} = \hat{n} \cdot \nabla \hat{n} = \frac{1}{B^2} \nabla_\perp \left(P + \frac{B^2}{2} \right), \quad \hat{n} = \frac{\mathbf{B}}{B}, \tag{12}$$

where $\nabla_\perp$ is the gradient perpendicular to the magnetic field and $\hat{n}$ is the unit vector along the field. From Eq. (12), another expression for the magnetic curvature can be obtained,

$$\boldsymbol{\kappa} = \hat{n} \cdot \nabla \hat{n} = \kappa_n \frac{\nabla \psi}{2\psi} + \kappa_g (\iota \nabla \zeta - \nabla \theta), \tag{13}$$

in which the magnetic curvature is decomposed in terms of the normal magnetic curvature κ_n, given by

$$\kappa_n = \frac{2\psi}{B^2} \frac{\partial}{\partial \psi} \left(P + \frac{B^2}{2} \right) - \frac{2\psi \tilde{\beta}}{B^3 \sqrt{g}} \left(\frac{\partial}{\partial \zeta} + \iota \frac{\partial}{\partial \theta} \right) B, \tag{14}$$

and the geodesic magnetic curvature κ_g, which is given by

$$\kappa_g = \frac{1}{B^3 \sqrt{g}} \left(I \frac{\partial}{\partial \zeta} - J \frac{\partial}{\partial \theta} \right) B, \quad \langle \kappa_g \rangle = 0. \tag{15}$$

Here brackets indicate a flux surface average, and $\tilde{\beta}$ is obtained by solving the following magnetic differential equation:

$$\mathbf{B} \cdot \nabla \tilde{\beta} = \frac{dP}{d\psi} \left(1 - \frac{B^2}{\langle B^2 \rangle} \right). \tag{16}$$

The contravariant form of the normal magnetic curvature, κ^n, is expressed as

$$\kappa^n = \frac{\boldsymbol{\kappa} \cdot \nabla \psi}{|\nabla \psi|^2} = \kappa_n + \kappa_g \frac{2\psi (J g_{\psi\theta} - I g_{\psi\zeta})}{\sqrt{g} |\nabla \psi|^2}. \tag{17}$$

In Figs. 4(d) and 5(d), the contravariant normal magnetic curvature κ^n is shown plotted along the magnetic field line. The phase due to the toroidicity and that due to the helicity are both quite evident. At the outer side of the torus, where $\eta = 2p\pi$ with p an integer, locally unfavorable magnetic curvature occurs near $\eta = 0$ and $\pm 4\pi$, but locally favorable curvature at $\eta = \pm 2\pi$. Because of such behavior, the local magnetic curvature is expected to have a strong dependence on the magnetic field line (i.e., on α). This sort of strong magnetic field line dependence (α-dependence) by the local magnetic curvature is a universal feature in heliotron/torsatron systems with appreciable helical ripple.

IV. STABILITY PROPERTIES

Before examining the stability properties of high-mode-number ballooning modes and the relation between high-mode-number and low-mode-number modes, we will present a brief summary of the global and local equilibrium characteristics. In addition, the last three points in this list summarize some other useful information.

1. The reduction or vanishing of the stabilization effect of the local magnetic shear $\hat{s}$ in the region of stellarator-like global magnetic shear is a universal feature, at least in $L = 2$ heliotron/torsatron systems with a large Shafranov shift. The dependence of $\hat{s}$ on the field line label α and on the type of pressure profile is weak, since the behavior of $\hat{s}$ is determined by toroidal force balance with a stellarator-like global magnetic shear, such as is inherent in $L = 2$ heliotron/torsatron systems.

2. As the value of β increases, the local shape of the flux surfaces as expressed by $|\nabla\psi|$ enhances the stabilizing effect from the secular term in $|\mathrm{k}_\perp|$ at the outer side of the torus, but reduces it at the inner side. The effect of local compression or decompression of flux surfaces on this stabilizing term, coming through toroidal force balance, is almost independent of α and the type of pressure profile. This, too, is a universal feature in $L = 2$ heliotron/torsatron systems with a large Shafranov shift.

3. As β increases, the stabilization from field line bending is significantly reduced within one poloidal period along the field line ($|\eta| < \pi$), but significantly enhanced farther out along the field line. This feature is due to the superposition of the preceding two characteristics in this summary list. This feature is universal, at least in $L = 2$ heliotron/torsatron systems with a large Shafranov shift.

4. A universal feature in heliotron/torsatron systems with appreciable helical ripple is that the local magnetic curvature at the outer side of the torus depends on α.

5. The pressure profile has a significant affect on the Mercier criterion because there is always an average magnetic hill near the plasma periphery. A peaked pressure profile leads to a slightly Mercier-unstable or a completely Mercier-stable equilibrium, whereas a broad pressure profile leads to a strongly Mercier-unstable equilibrium.

6. In the high-mode-number ballooning equation, typically there are three spatial scale lengths along the magnetic field line. For strong global shear, these scale lengths have the following ordering,

$$1 \gg \frac{1}{s} \gg \frac{\tau}{M},$$

whereas for weak global shear, these scale lengths are ordered as follows,

$$\frac{1}{s} \gg 1 \gg \frac{\tau}{M}.$$

Here, 1 and $\frac{\tau}{M}$ are the scale lengths determined by the toroidicity and the helicity, respectively, while the scale length $\frac{1}{s}$ arises from the secular term in the local magnetic shear integrated along the magnetic field line, given by Eq. (9).

7. In the integrated local magnetic shear , which appears in the perpendicular wavenumber, given in Eq. (10), the scale length due to the toroidicity determines the typical scale of its envelope around the secular term having the scale length of $\frac{1}{s}$, while its rapid modulation is due to the helicity.

8. The normal and geodesic components of the magnetic curvatures have variations both on the toroidicity scale length and also on the helicity scale length.

9. The parameter D_M that describes the Mercier criterion is derived from an asymptotic analysis of the exact high-mode-number ballooning mode equation with zero frequency. For equilibria that are Mercier stable, the high-mode-number ballooning equation has solutions that decay along the magnetic field line in the asymptotic region, i.e., where

$\eta - \theta_k \gg 0$. On the other hand, Mercier-unstable equilibria correspond to solutions of the high-mode-number ballooning equation that have oscillatory asymptotic behavior along the field line.

10. Ballooning modes with large growth rates tend to be localized along the field line. (This feature can be easily understood from the variational form for the high-mode-number ballooning equation.) On the other hand, modes near marginal stability tend to be extended along the field line.

11. A crucial difference between a heliotron/torsatron system and a tokamak is the dependence of equilibrium quantities on the field line label α in covering space (ψ, η, α) for the former. In a helical system, the eigenfunctions for high-mode-number ballooning modes depend on the poloidal angle η in the three-dimensional parameter space (ψ, θ_k, α), and hence the corresponding eigenvalues depend on the three parameters (ψ, θ_k, α). By contrast, the eigenfunctions in a tokamak depend on η in the two-dimensional parameter space (ψ, θ_k), and thus the corresponding eigenvalues depend on only two parameters (ψ, θ_k).

High-mode-number ballooning modes are described by the following equation[5]:

$$\frac{\partial}{\partial \eta}\left[|\mathbf{k}_\perp|^2 \frac{\partial}{\partial \eta}\Phi\right] + \Omega^2 \left(\frac{\langle B^2 \rangle}{B^2}\right)^2 |\mathbf{k}_\perp|^2 \Phi + \frac{2}{B_0}\left(\frac{J + \iota I}{\iota B}\right)^2 \frac{dP}{d\psi}\left[\kappa^n - \kappa_g \int^\eta \hat{s} d\eta\right]\Phi = 0, \tag{18}$$

where $\Omega = \omega \tau_A$ is the eigenfrequency normalized by the Alfven time τ_A, which is given by

$$\tau_A^2 = \frac{\rho_m}{\left(2\pi \frac{\iota d\Phi_T}{dV}\right)^2}. \tag{19}$$

Other quantities used in Eq. (18) are defined in Eqs. (7)–(17). For a currentless equilibrium, we set $I = 0$ in Eq. (18).

We will numerically solve Eq. (18) in the covering space (ψ, η, α), which is related to the Boozer coordinate system (ψ, θ, ζ) by Eq. (6). The boundary condition used for the numerical solution of Eq. (18) is $\Phi = 0$ at $|\eta - \theta_k| = p \times 2\pi$, where the choice of the appropriate value for the integer p depends on the convergence properties of the eigenfunctions for various parameters. For modes localized along a field line, we typically used $p = 4$. For modes with extended structure along a field line, we typically used $p = 32$. After having obtained a solution with eigenvalue Ω_0^2, we slightly reduced the position of the boundary, say, by $\delta p = j \times 0.05$ with $j = 1, 2, \cdots$, and again obtained the solution, with corresponding eigenvalue Ω_j^2. Then, if the difference $\delta\Omega_j^2 \equiv \frac{|\Omega_0^2 - \Omega_j^2|}{\Omega_0^2}$ is smaller than 10^{-8}, we treated Ω_0^2 as the true eigenvalue. To solve Eq. (18), we usually used the sixth-order Runge-Kutta numerical method. Occasionally the Adams method was used to check the solutions obtained by means of the sixth-order Runge-Kutta method.

To calculate the equilibria, the VMEC code[7] was used, with fixed boundary conditions, for 121 radial grids and 7 poloidal harmonics (with mode numbers $m = 0 \sim 6$) and 13 toroidal harmonics (with mode numbers $n = -6 \sim 6$). The transformation from the VMEC magnetic coordinate system to the Boozer magnetic coordinate system was carefully carried out with the use of Eqs. (22) and (25) of Ref. 1. In order to carry out this transformation with precision, 120 poloidal harmonics (with mode numbers $m = 0 \sim 119$) and 25 toroidal harmonics (with mode numbers $n = -12 \sim 12$) were used in the Boozer coordinate system. As was described in Ref. 1, the poloidal angle of the VMEC coordinate system is an optimized angle, which is similar to the poloidal angle proportional to the arc length ("uni-arc angle"), whereas the toroidal angle of the VMEC coordinate system is simply the geometrical toroidal angle. Because the poloidal angle of the Boozer coordinate system is greatly deformed from the uni-arc poloidal angle near the shearless region (cf. Figs. 2 and 3), many harmonics are needed. The toroidal angle of the Boozer coordinate system, however, is very similar to the usual geometrical toroidal angle in a planar-axis heliotron/torsatron system, and hence a

small number of toroidal harmonics is sufficient. The maximum relative errors in B and R due to the transformation at the grid points are approximately 10^{-7} and 10^{-9}, respectively.

The basic domain for the (ψ, θ_k, α) space is $\psi_{\min} \leq \psi \leq \psi_{\max}$ or $(0 \leq \psi_N \leq 1)$, $-\pi \leq \theta_k \leq \pi$, and $0 \leq \alpha \leq \frac{2\pi}{M}$. Note that a heliotron/torsatron equilibrium with M as the toroidal pitch number of the helical coils have an M-fold periodicity in the toroidal direction, with the basic domain for α correspondingly reduced. All of the numerical calculations described in the present paper are performed in this basic domain.

A. Equilibria that are strongly Mercier-unstable

Figure 6 shows the variation with α and the ψ-dependence of the unstable eigenvalues Ω^2, with $\theta_k = 0$, for the broad pressure profile given by Eq. (2) with $\beta_0 = 4\%$. This equilibrium has flux surfaces that are strongly Mercier-unstable, as seen in Fig. 1. A comparison of Fig. 6 with the graphs for D_M in Fig. 1 shows that the region unstable with respect to high-mode-number ballooning modes radially overlaps the Mercier-unstable region. Also, when we compare Fig. 6 with the graphs for s in Fig. 1, we find that these high-mode-number modes are located in the region where the global magnetic shear is stellarator-like. In Fig. 6, the open circles indicate eigenvalues $\Omega^2(\psi_N, \theta_k = 0, \alpha = 0)$ where the chosen field line with $\alpha = 0$ passes through the place where the magnetic curvature is locally most unfavorable, i.e., on the outer side of the torus at $\eta = 0$ in a horizontally elongated poloidal cross section. The open squares in Fig. 6 indicate eigenvalues $\Omega^2(\psi_N, \theta_k = 0, \alpha = \frac{\pi}{M})$ where the selected field line with $\alpha = \frac{\pi}{M}$ passes through the point where the magnetic curvature is locally most favorable, i.e., on the outer side of the torus at $\eta = 0$ in a vertically elongated poloidal cross section.

For parameters such that the high-mode-number ballooning modes are marginally stable, the α-dependence of the eigenvalues Ω^2 is so weak that high-mode-number ballooning modes can become unstable even in the region where the magnetic curvature is locally most

favorable, i.e., $\alpha = \frac{\pi}{M}$. In particular, the α-dependence is quite weak in the region $\psi_N = 0.35 \sim 0.45$ where the global shear is small. The eigenfunction $\Phi(\psi_N = 0.39, \theta_k = 0, \alpha = 0)$ obtained from Eq. (18) in this region is shown in the top graph of Fig. 7. The modulation due to the toroidicity is evident, but there is almost no perceptible affect due to the helicity. Since the condition $\frac{1}{s} > 1$ is satisfied in this region, i.e., the scale length for the secular stabilizing term in $|\mathbf{k}_\perp|$ that arises from the global magnetic shear s is longer than that due to the toroidicity, the eigenfunction Φ has a considerably extended structure along the magnetic field line, extending over regions where the magnetic curvature is both locally unfavorable and favorable (in terms of the toroidicity). The structure of the eigenfunction has several peaks on the outer side of the torus, reflecting the toroidicity scale length in the local magnetic curvature. This type of extended structure with several peaks on the outer side of the torus indicates that high-mode-number modes with $\alpha = \frac{\pi}{M}$ experience destabilization from adjacent regions of locally unfavorable magnetic curvature region at the outer side of the torus—which in turn leads to the α-dependence of Ω^2 being weak. High-mode-number ballooning modes being nearly marginally stable in the region where the global magnetic shear is weak have a correspondence to weakly ballooning modes in tokamaks.[5]

Near marginal stability, in the region ($\psi_N = 0.7 \sim 0.8$) where the global magnetic shear is relatively strong, the toroidicity scale length is larger than that due to the global magnetic shear in the secular term: i.e., $1 > \frac{1}{s}$. In this case, the eigenfunction Φ has a localized structure, with little oscillatory behavior, as shown in the bottom graph in Fig. 7. This type of localized structure prevents the eigenmode from experiencing destabilization at adjacent regions on the outer side of the torus where the magnetic curvature is locally unfavorable, and hence the α-dependence of Ω^2 becomes stronger than in the case when the global magnetic shear is low. Eigenfunctions that are near marginal stability with $0 > \Omega^2 > \min \Omega^2(\psi_N, \theta_k = 0, \alpha = \frac{\pi}{M})$ have extended structures along the magnetic field line, and the α-dependence of their eigenvalues is so weak that the domain of unstable eigenvalues is unbounded with

respect to α. Then, since the unstable eigenvalues are bounded in both ψ and θ_k, the level surfaces for the eigenvalues are topologically cylindrical in (ψ, θ_k, α) space.

Away from marginal stability, the α-dependence of the eigenvalues Ω^2 becomes fairly strong. This can be seen in Fig. 6 where cross points indicate the α-dependence of the most unstable eigenvalue $\Omega^2(\psi_N = 0.66, \theta_k = 0, \alpha)$ plotted for the several values $\alpha = \frac{j}{5}\frac{\pi}{M}$ for $j = 0, 1, \cdots, 5$. The scale length for the global magnetic shear in the secular term is smaller than that for the toroidicity: i.e., $1 > \frac{1}{s}$. A typical eigenfunction $\Phi(\psi_N = 0.66, \theta_k = 0, \alpha = 0)$ is shown in the middle graph of Fig. 7. The rather localized non-oscillatory structure of this eigenfunction results from the $1 > \frac{1}{s}$ ordering of the different scale lengths. Localized high-mode-number ballooning modes such as this, which are not near marginal stability, have a correspondence to strongly ballooning modes in tokamaks, apart from the strong dependence on α. Since high-mode-number ballooning modes with large growth rates, i.e., $\Omega^2 < \min \Omega^2(\psi_N, \theta_k = 0, \alpha = \frac{\pi}{M})$, tend to be localized along field lines, their strong α-dependence causes the domain of unstable eigenvalues to be bounded with respect to α, and hence the level surfaces for the eigenvalues in (ψ, θ_k, α) space are topologically spheroidal. Otherwise, these strongly localized ballooning modes would be destabilized even in the region where the magnetic curvature is locally favorable, if the eigenfrequency ω^2 has week dependence on α.

Our numerical results show that the more highly localized the eigenfunctions are, the stronger their α-dependence becomes, which causes the level surfaces for the eigenvalues to be transformed topologically from being cylindrical to being spheroidal.

B. Equilibria that are slightly Mercier-unstable or completely Mercier-stable

For the peaked pressure profile of Eq. (1) with $\beta_0 = 4\%$, the high-mode-number ballooning modes are found to be completely stable, even though this equilibrium is slightly

Mercier unstable, as shown in Fig. 1. When β_0 goes up to about 6%, the high-mode-number ballooning modes become unstable, whereas the Mercier modes are only slightly unstable. The equilibrium with $\beta_0 = 8\%$ is completely Mercier stable; i.e., it has a second stability regime with respect to interchange modes. The high-mode-number ballooning modes, however, are more unstable with $\beta_0 = 8\%$ than with $\beta_0 \sim 6\%$. The ψ-dependence of the stable and unstable eigenvalues Ω^2 with $\theta_k = 0$ and $\alpha = 0$ is shown in Fig. 8 for the peaked pressure profile with $\beta_0 = 8\%$. The growth rates are quite large; i.e., these high-mode-number modes are strongly ballooning modes apart from their significant α-dependence. A comparison of Fig. 8 with the graphs for s of Fig. 1 shows that these modes become unstable in the region where the global magnetic shear is stellarator-like.

The eigenfunction corresponding to the most unstable eigenvalue, viz., $\Phi(\psi_N = 0.56, \theta_k = 0, \alpha = 0)$, is shown in the middle graph of Fig. 9. Since the scale length for the global magnetic shear is smaller than that for the toroidicity and because the typical growth rates are very large, the eigenfunction is highly localized along the magnetic field line. This localized structure along the field line does not change for unstable eigenfunctions near the marginal stability of high-mode-number ballooning modes. Moreover, even the stable eigenfunctions in the vicinity of the marginal stability, shown in the top and the bottom graphs of Fig. 9, have a highly localized structure, similar to that shown in the middle graph of Fig. 9, i.e., regardless the sign and magnitude of the eigenvalues the eigenfunctions of the discrete modes have a highly localized structure.

These stable eigenfunctions are considered to correspond to high-mode-number TAE modes (toroidicity-induced shear Alfvén eigenmodes). The asymptotic form of the Shrödinger-type of the high-mode-number ballooning equation at $|\eta| \to \infty$ is

$$\frac{\partial^2 \widehat{\Phi}}{\partial \eta^2} + \left[\Omega^2 \left(\frac{\langle B^2 \rangle}{B^2} \right)^2 - U(\Omega^2, \eta) \right] \widehat{\Phi} = 0, \tag{20}$$

where the eigenfunction of the Shrödinger-type of the equation and the asymptotic potential

are, respectively, given by

$$\widehat{\Phi} = \Phi|\mathrm{k}_\perp|, \tag{21}$$

$$U(\Omega^2, \eta) = \frac{1}{|\nabla\psi|}\frac{\partial^2|\nabla\psi|}{\partial\eta^2}. \tag{22}$$

From the solution of Eq. (20) we can understand the boundaries between spectral gaps and the Alfvén continuum. The modulation of flux surfaces due to a large Shafranov shift, expressed by $|\nabla\psi|$, is noticeable as shown in Fig. 4(b). Since a large Shafranov shift enhances the Fourier components with phases of toroidicity, ellipticity, and triangularity in $|\nabla\psi|$, the first, second, and third spectral gaps become quite large. Thus, the width of the Alfvén continuum between spectral gaps becomes quite narrow. The rather narrow width of the first Alfvén continuum between $\Omega^2 = 0$ and the lower boundary of the first gap leads to very small eigenvalues for the descrete stable eigenmodes (TAE modes) near the lower boundary of the first gap, as shown in Figs. 8 and 9. Also, the rather narrow width of the second Alfvén continuum between the first and the second spectral gaps leads to a large variation of the eigenvalues of high-mode-number TAE modes, shown in Fig. 8. The overall structure of the eigenfunctions for high-mode-number TAE modes is quite similar to that for high-mode-number ballooning modes, except that the former becomes negative at $|\eta| = 2\pi$, which is somewhat difficult to distinguish in Fig. 9. This structure reflects the typical periodicity of high-mode-number TAE modes, namely, 4π. More detailed explanation of the high-mode-number TAE modes and their relationship to high-mode-number ballooning modes will be presented in a separate publication.

The top graph in Fig. 10 shows the θ_k-and ψ-dependences of the eigenvalues Ω^2 for $\alpha = 0$. The calculation area is $0.422 \leq \psi_N \leq 0.791$ and $-0.03 \leq \frac{\theta_k}{2\pi} \leq 0.03$ The area indicated by the thick closed curves corresponds to the contours for the negative eigenvalues of high-mode-number ballooning modes, and the area indicated by the thin unclosed curves to the contours for the positive eigenvalues of high-mode-number TAE modes. Note that the unstable region

in θ_k is very narrow. The lower graph of Fig. 10 shows the θ_k-and α-dependences of the most unstable eigenvalue Ω^2 on the flux surface $\psi_N = 0.56$. The contours indicated by thick curves, centered at $\frac{\alpha}{2\pi/M} = 0, 1,$ and 2, correspond to the negative eigenvalues of high-mode-number ballooning modes. In contrast, the contours indicated by thin curves, centered at $\frac{\alpha}{2\pi/M} = 0.5$ and 1.5, correspond to the positive eigenvalues of high-mode-number TAE modes. Due to their highly localized structure along the field line, the high-mode-number ballooning modes alternate between instability and stability as α is varied, and consequently the level surfaces for the unstable eigenvalues have the topological form of spheroids in (ψ, θ_k, α) space.

In a slightly Mercier-unstable or completely Mercier-stable equilibrium, there are no cylindrical level surfaces of $\Omega^2(\leq 0)$ that exist near marginal stability surrounding the spherical level surfaces of $\Omega^2(< 0)$ in a strongly Mercier-unstable equilibrium. The reason for this is as follows: In a slightly Mercier-unstable or completely Mercier-stable equilibria with a peaked pressure profile, the destabilization of high-mode-number ballooning modes is weak compared with that for a strongly Mercier-unstable equilibria for which the maximum of the pressure gradient is located in the Mercier-unstable region. Thus, high-mode-number ballooning modes in a slightly Mercier-unstable or completely Mercier-stable equilibrium with a peaked pressure profile begins to become unstable after the stabilization is suppressed through a large Shafranov shift due to significant compression or decompression of the flux surfaces at the outer side or inner side, respectively, of the torus. Thus, the perpendicular wavenumber $|\mathbf{k}_\perp|$ becomes quite small within the poloidal region $|\eta| \leq 2\pi$, partially due to the reduction or vanishing of the stabilizing effect of the local magnetic shear near $\eta = 0$, and partially due to the reduction of the secular stabilizing term in $|\mathbf{k}_\perp|$ near $|\eta| = \pi$ on account of $|\nabla\psi|$ being considerably reduced. In contrast, the secular stabilizing term in $|\mathbf{k}_\perp|$ is much enhanced near $|\eta| = 2\pi$ by the increase in $|\nabla\psi|$. Therefore, it follows that the eigenfunctions of the unstable high-mode-number ballooning modes are localized within $|\eta| = 2\pi$

even for eigenvalues near marginal stability. This leads to such a strong α-dependence of the eigenvalue Ω^2 that the level surfaces for $\Omega^2(\leq 0)$ become spheroids. In other words, unstable eigenvalues do not have cylindrical level surfaces, and the spheroidal level surfaces for unstable eigenvalues are immediately surrounded by stable eigenvalues $\Omega^2 > 0$ of high-mode-number TAE modes. In contrast, high-mode-number ballooning modes in a strongly Mercier-unstable equilibria with a broad pressure profile become unstable before the stabilizing effects are suppressed. Thus, the eigenfunctions do not have a localized structure, which leads to a weak α-dependence of the eigenvalue Ω^2, and consequently the cylindrical level surfaces for Ω^2 (≤ 0) exist near the magninal stability.

The spectrum of the eigenvalues $\Omega^2(\psi_N, \theta_k, \alpha)$ can be expressed as[3]

$$\Omega^2 = \sum_{m,n} \Omega^2_{m,n}(\psi_N) \cos(m\theta_k + n\zeta_k), \tag{23}$$

with $\zeta_k = \alpha + q\theta_k$. The spectrum for the particular eigenvalue $\Omega^2(\psi_N = 0.56, \theta_k, \alpha)$ is shown in Fig. 11. One contribution to the spectrum comes from the toroidicity (the $n = 0$ components). The other contribution comes from the helicity (the $n \neq 0$ components). Among the $n = 0$ components due to the toroidicity, $\Omega^2_{0,0}$, $\Omega^2_{1,0}$ and $\Omega^2_{2,0}$ are positive (i.e., stable), while most of the negative (i.e., unstable) contribution comes from the broad spectrum of higher harmonics with $m \geq 3$. The dominant components due to the helicity (namely, the components with $n = 10$) have a broad spectrum in m and contribute a significant negative (unstable) contribution, thus indicating a strong α-dependence of the eigenvalues. The broad spectrum with respect to m indicates that the width in θ_k of the level surfaces for ω^2 is very narrow.

C. Stability properties of high-mode-number modes and their relationship to low-mode-number modes

We can now categorize the high-mode-number ballooning modes in heliotron/torsatron systems into two types and investigate their properties.[3] One type of high-mode-number

ballooning mode has level surfaces for its unstable eigenvalues Ω^2 that are topologically cylindrical in (ψ, θ_k, α) space. This type of high-mode-number ballooning mode occurs only near Mercier marginal stability in an equilibrium that is strongly Mercier-unstable due to a broad pressure profile. The high-mode-number modes that have small growth rates are significantly extended along a magnetic field line, extending over several poloidal periods with locally unfavorable and favorable magnetic curvature regions at the outer side of the torus.

The other type of high-mode-number ballooning mode has level surfaces for the unstable eigenvalues Ω^2 that are topologically spheroidal in (ψ, θ_k, α) space. These high-mode-number modes arise in two different ways. For a strongly Mercier-unstable equilibrium with a broad pressure profile, this type of mode occurs in the strongly Mercier-unstable region, far from marginal stability. It follows that the spheroidal level surfaces of the eigenvalues are surrounded by the cylindrical level surfaces for the unstable eigenvalues in (ψ, θ_k, α) space. For a slightly Mercier-unstable or completely Mercier-stable equilibrium with a peaked pressure profile, only this type of high-mode-number mode occurs, so that the spheroidal level surfaces for the unstable eigenvalues are surrounded in (ψ, θ_k, α) space by the level surfaces for the stable eigenvalues of high-mode-number TAE modes. The high-mode-number modes with large growth rates are extremely localized along a magnetic field line.

In order to examine the global structure of the high-mode-number ballooning modes, the eikonal $S(\psi, \alpha)$ must be specified on a level surface for Ω^2 in (ψ, θ_k, α) space. Doing so leads to information about the low-mode-number ballooning modes. For this purpose, the method of characteristics will be used. Hence, the following ray equations will be solved[3]:

$$\dot{\alpha} = -\theta_k \frac{\partial \lambda}{\partial \theta_k}, \tag{24}$$

$$\dot{q} = \frac{\partial \lambda}{\partial \theta_k}, \tag{25}$$

$$\dot{\theta}_k = \theta_k \frac{\partial \lambda}{\partial \alpha} - \frac{\partial \lambda}{\partial q}, \tag{26}$$

Hereafter, the safety factor q will be used instead of ψ. In Eqs. (23)–(25), $\dot{\alpha}$ denotes the derivative with respect to a dummy time variable that parameterizes the characteristics. Also, the function λ represents the dispersion relation:

$$\lambda = \omega^2(q, \theta_k, \alpha). \tag{27}$$

The eikonal S is constant along a ray trajectory.

Since the unstable eigenvalues ($\omega^2 < 0$) are bounded in θ_k, the poloidal periodicity requirement on the eikonal is satisfied.[3] Thus, unstable eigenvalues with cylindrical level surfaces in (q, θ_k, α) space must satisfy both the requirement that the eikonal S have toroidal periodicity and also the requirement that it be single-valued in q. These requirements lead to a quantization condition, from which the toroidal mode number of the ballooning modes is determined. For high-mode-number modes whose eigenvalues have cylindrical level surfaces, a tokamak-like treatment can be applied to determine the global radial structure and the typical toroidal mode number. Furthermore, high-mode-number modes of this sort will be continuously connected to low-mode-number ballooning modes.[4]

On the other hand, high-mode-number ballooning modes whos eigenvalues have spheroidal level surfaces are essentially three-dimensional in nature. Since both the poloidal and toroidal periodicity requirements are satisfied, there remains only the requirement of single-valuedness in q. Thus, the toroidal mode number is not a good quantum number, even in an approximate sense. Moreover, being bounded in α implies that these high-mode-number modes never connect to low-mode-number modes. At least one stable fixed point (a sink) and one unstable fixed point (a source) exist on the spheroid, which are obtained from the solution of Eqs. (23)–(25) with $\dot{\alpha} = \dot{q} = \dot{\theta}_k = 0$. The ray must spiral out of an unstable fixed point and into a stable fixed point, whose eigenvalue corresponds to an unstable continuum band.[3]

The spheroids are highly elongated in α and highly contracted in θ_k, as shown in Fig. 10. From the following equation,

$$\frac{d\alpha}{dq} = -\theta_k, \tag{28}$$

obtained from the combination of Eqs. (23) and (24), it can be expected that the change in α for a single rotation in both the θ_k and the q directions is quite small.

These considerations concerning high-mode-number ballooning modes whose eigenvalues have spheroidal level surfaces of eigenvalues in (ψ, θ_k, α) space indicate that finite-mode-number ballooning modes should be expected to have the following stability properties: Finite-mode-number modes will be excited in the region of locally unfavorable magnetic curvature between adjacent helical coils at the outer side of the torus. The minimum toroidal mode number to be expected is at least M, since a helical device with a toroidal pitch number M has M periods in the toroidal direction. To be localized both toroidally and poloidally, toroidal mode numbers M, $2M$, $3M$, $4M$, $\cdots$ are needed. Hence, finite Larmor radius effects that can have a stabilizing effect on finite-mode-number ballooning modes become significant, say, for $M \geq 10$.

V. DISCUSSION

The stability properties of high-mode-number ballooning modes and their relationship to low-mode-number modes has been examined in an $L = 2/M = 10$ heliotron/torsatron; here, L and M are the polarity and the toroidal pitch number of the helical coils, respectively. The exact incompressible high-mode-number ballooning mode equation was solved in the covering space (ψ, η, α) for three-dimensional equilibria, where ψ and α are the flux surface and the magnetic field line labels, respectively, and η is the coordinate along the magnetic field line $(-\infty < \eta < \infty)$. In heliotron/torsatron systems, the eigenvalues ω^2 are a function of ψ, θ_k, and α, with θ_k the radial wavenumber from the eikonal analysis, whereas in a tokamak

plasma the eigenvalues are not functions of α. Thus, the properties of high-mode-number ballooning modes in heliotron/torsatron systems are mainly clarified by the magnetic field line dependence of their eigenvalues ω^2.

In a heliotron/torsatron system with a large Shafranov shift, at relatively low-β values the large Shafranov shift reduces or cancels the stabilizing effect due to the local magnetic shear at the outer side of the torus, even in the region where the global magnetic shear is stellarator-like, and when strong compression of the flux surfaces due to the Shafranov shift enhances the secular stabilizing part of the local shear at the outer side of the torus, while strong flux surface decompression reduces it at the inner side. The superposition of these effects leads to significant suppression of the stabilizing effects due to the perpendicular wavenumber within the first poloidal period along the magnetic field line, and enhancement at $|\eta| = 2\pi$.

Broad pressure profiles lead to a highly Mercier-unstable equilibrium, with the maximum pressure gradient located within the Mercier-unstable region. In contrast, peaked pressure profiles lead to a slightly Mercier-unstable or completely Mercier-stable equilibrium, with the maximum pressure gradient located within the Mercier stable region. Thus, it is easier for high-mode-number ballooning modes to occur in equilibria with broad pressure profiles than in equilibria with peaked pressure profiles. In other words, the β value at which high-mode-number modes occur in an equilibrium with a broad pressure profile is lower than that in an equilibrium with a peaked pressure profile.

In highly Mercier-unstable equilibria with broad pressure profiles, the high-mode-number ballooning modes are destabilized before the stabilizing effects within a single poloidal period along a field line are much suppressed by the Shafranov shift. Here, high-mode-number modes have an extended interchange-like structure along a magnetic field line. Although the destabilizing effects have a strong dependence on the magnetic field line (i.e., α-dependence) at the outer side of the torus due to the helicity of the external coil system, the extended

structure of the eigenmodes along the field line relaxes the α-dependence to such an extent that near marginal stability, high-mode-number modes become tokamak-like, with eigenvalues $\omega^2 \sim \omega^2(\psi, \theta_k)$, where ψ and θ_k are the flux surface label and the radial wavenumber, respectively.

In contrast, in a slightly Mercier-unstable or completely Mercier-stable equilibrium, created by a peaked pressure profile like that used in standard stability analyses or normally observed in CHS experiments,[8] the high-mode-number ballooning modes are destabilized after the stabilizing effects within a single poloidal period along a magnetic field line are sufficiently suppressed by the Shafranov shift. Thus, these modes are highly localized within one poloidal period, and this leads to such a strong α-dependence that the level surfaces for $\omega^2(\psi, \theta_k, \alpha)$ (≤ 0) become spheroidal in (ψ, θ_k, α) space. Highly localized modes like these with the spheroidal level surfaces for ω^2 never connect to low-mode-number modes. In configuration space, these modes are so highly localized within each toroidal pitch of the helical coils that they may experience significant finite Larmor radius stabilization.

Finite Larmor Rradius stabilizing effects on high-mode-number ballooning modes whose eigenvalues have spheroidal level surfaces will be considered in a future publication.

A. ACKNOWLEDGMENTS

The author expresses his gratitude to Professors M. Okamoto and T. Sato of the National Institute for Fusion Science and to Professor R.D. Hazeltine of the Institute for Fusion Studies for their interest in and encouragement of this work. The author also would like to thank Professors H.L. Berk and J.W. Van Dam of the IFS for fruitful discussions and their interest in this work.

The author's work was supported by AFOSR grant F49620-95-1-0529 through the Japan Industry and Management of Technology (JIMT) Program at the IC^2 Institute, The University of Texas at Austin. It was also partially supported by the U.S. Department of Energy

under contract DE-FG03-96ER-54346 with the Institute for Fusion Studies. The author's visit was arranged through the U.S.-Japan Joint Institute for Fusion Theory exchange program.

References

[1] N. Nakajima, submitted to Phys. Plasmas.

[2] A. Iiyoshi, M. Fujiwara, O. Motojima, N. Oyabu, and K. Yamazaki, Fusion Technol. **17**, 148 (1990).

[3] R.L. Dewar and A.H. Glasser, Phys. Fluids **26**, 3038 (1983).

[4] W.A. Cooper, D.B. Singleton, and R.L. Dewar, Phys. Plasmas **3**, 275 (1996).

[5] R.D. Hazeltine and J.D. Meiss, Phys. Reports **121**, 1 (1985).

[6] K. Ichiguchi, N. Nakajima, M. Okamoto, Y. Nakamura, and M. Wakatani, Nucl. Fusion **33**, 481 (1993).

[7] S.P. Hirshman, Phys. Fluids **26**, 3553 (1983).

[8] S. Okamura, K. Matsuoka, K. Nishimura, K. Tsumori, R. Akiyama, S.Sakakibara, H. Yamada, S. Morita, T. Morisaki, N. Nakajima, K. Tanaka, J. Xu, K. Ida, H. Iguchi, A. Lazaros, T. Ozaki, H. Arimoto, A. Ejiri, M. Fujiwara, H. Idei, O. Kaneko, K. Kawahata, T. Kawamoto, A. Komori, S. Kubo, O. Motojima, V.D. Pustovitov, C. Takahashi, K. Toi, and I. Yamada, Nucl. Fusion **35**, 283 (1995).

[9] J.M. Greene, J.L. Johnson, Plasma Phys. **10**, 729 (1968).

[10] A.H. Boozer, Phys. Fluids **23**, 904 (1980).

FIGURE CAPTIONS

FIG. 1. Global rotational transform ι, global magnetic shear s, average magnetic well index V'', and Mercier criterion parameter D_M, all as functions of the normalized toroidal flux $\psi_N = \frac{\psi}{\psi_{\rm edge}}$: The upper graphs are for the peaked pressure profile of Eq. (1), and the lower graphs for the broad pressure profile of Eq. (2). The dotted, dot-dashed, and solid curves in both upper and lower graphs correspond to $\beta_0 = 0, 4$, and 8%, respectively. Note that negative (positive) V'' means the existence of an average magnetic well (hill), and that $D_M > 0$ implies Mercier stability.

FIG. 2. Equally spaced (ψ, θ) mesh in the Boozer coordinate system (ψ, θ, ζ) on a horizontally elongated poloidal cross section: The upper graphs are for the peaked pressure profile of Eq. (1), and the lower graphs for the broad pressure profile of Eq. (2). The left-hand upper and lower graphs have $\beta_0 = 0$, the middle graphs $\beta_0 = 4\%$, and the right-hand graphs $\beta_0 = 8\%$. The direction of the poloidal angle θ and of the magnetic field lines is clockwise. The position of $\theta = 0$ is on the equatorial plane at the outer side of the torus.

FIG. 3. Same quantities as shown in Fig. 2, but on a vertically elongated poloidal cross section.

FIG. 4. Variation along a magnetic field line of (a) the integrated local shear $\left[\int^{\eta} \widehat{s} d\eta\right]^2$, with the quantity $(s\eta)^2$ shown for reference (thin curve); (b) the flux surface shape quantity $\frac{|\nabla\psi|^2}{2\psi B_0}$, with the quantity $\frac{|\nabla\psi|^2}{2\psi B_0} = 1$ shown for reference (thin dotted curve); (c) the square of the perpendicular wavenumber $|\mathrm{k}_\perp|^2$; and (d) the contravariant normal magnetic curvature κ^n. These quantities are shown at $\psi_N = 0.56$, $\theta_k = 0$, and $\alpha = 0$ for an equilibrium with a peaked pressure profile with $\beta_0 = 8\%$. The

position $\eta = 0$ is the outer midplane location for the torus. The most unstable eigenvalue on the chosen field line occurred when $\theta_k = 0$ (See Fig. 8, middle graph of Fig. 9 and Figs. 10 and 11).

FIG. 5. The same quantities as shown in Fig. 4, plotted along the magnetic field line at $\psi_N = 0.39$, $\theta_k = 0$, and $\alpha = 0$, for an equilibrium with a broad pressure profile with $\beta_0 = 4\%$. The position $\eta = 0$ is the outer midplane location for the torus. On the chosen field line, eigenvalues near marginal stability occurred when $\theta_k = 0$ (See Fig. 6 and top graph of Fig. 7).

FIG. 6. The α-and ψ-dependence of the eigenvalue Ω^2, with $\theta_k = 0$, for the broad pressure profile of Eq. (2) with $\beta_0 = 4\%$. The open circles denote $\Omega^2(\psi_N, \theta_k = 0, \alpha = 0)$ and the open squares $\Omega^2(\psi_N, \theta_k = 0, \alpha = \frac{\pi}{M})$. The cross points denote $\Omega^2(\psi_N = 0.66, \theta_k = 0, \alpha = \frac{j}{5}\frac{\pi}{M})$ for $j = 0, 1, \cdots, 5$.

FIG. 7. High-mode-number ballooning mode eigenfunctions $\Phi(\psi_N, \theta_k = 0, \alpha = 0)$ for a strongly Mercier-unstable equilibrium with the broad pressure profile of Eq. (2) with $\beta_0 = 4\%$: (a) top graph at $\psi_N = 0.39$; (b) middle graph at $\psi_N = 0.66$; and (c) bottom graph at $\psi_N = 0.79$.

FIG. 8. The ψ-dependence of the eigenvalue Ω^2, with $\theta_k = 0$ and $\alpha = 0$, for the peaked pressure profile of Eq. (1) with $\beta_0 = 8\%$.

FIG. 9. Eigenfunctions $\Phi(\psi_N, \theta_k = 0, \alpha = 0)$ for a completely Mercier-stable equilibrium with the peaked pressure profile of Eq. (1) with $\beta_0 = 8\%$: (a) top graph at $\psi_N = 0.42$; (b) middle graph at $\psi_N = 0.56$; and (c) bottom graph at $\psi_N = 0.79$. The top and bottom eigenfunctions correspond to high-mode-number TAE modes. The middle eigenfunction is a high-mode-number ballooning mode.

FIG. 10. (a) The θ_k and ψ-dependence of the eigenvalue Ω^2, with $\alpha = 0$, and (b) the θ_k and α-dependence of the most unstable eigenvalue Ω^2, with $\psi_N = 0.56$, both for the peaked pressure profile of Eq. (1) with $\beta_0 = 8\%$.

FIG. 11. Spectrum of the eigenvalue $\Omega^2(\psi_N = 0.56, \theta_k, \alpha)$.

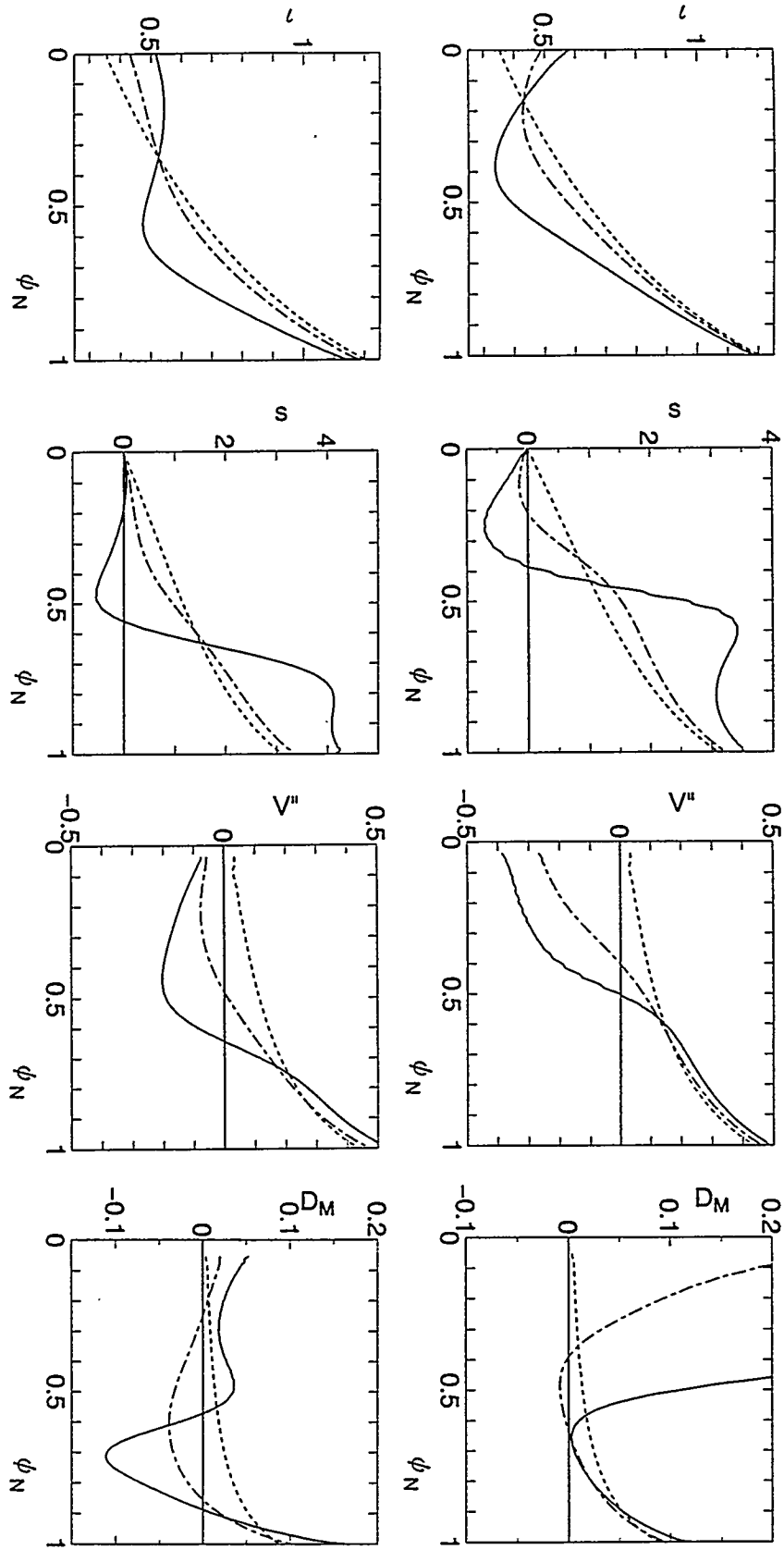

Fig. 1

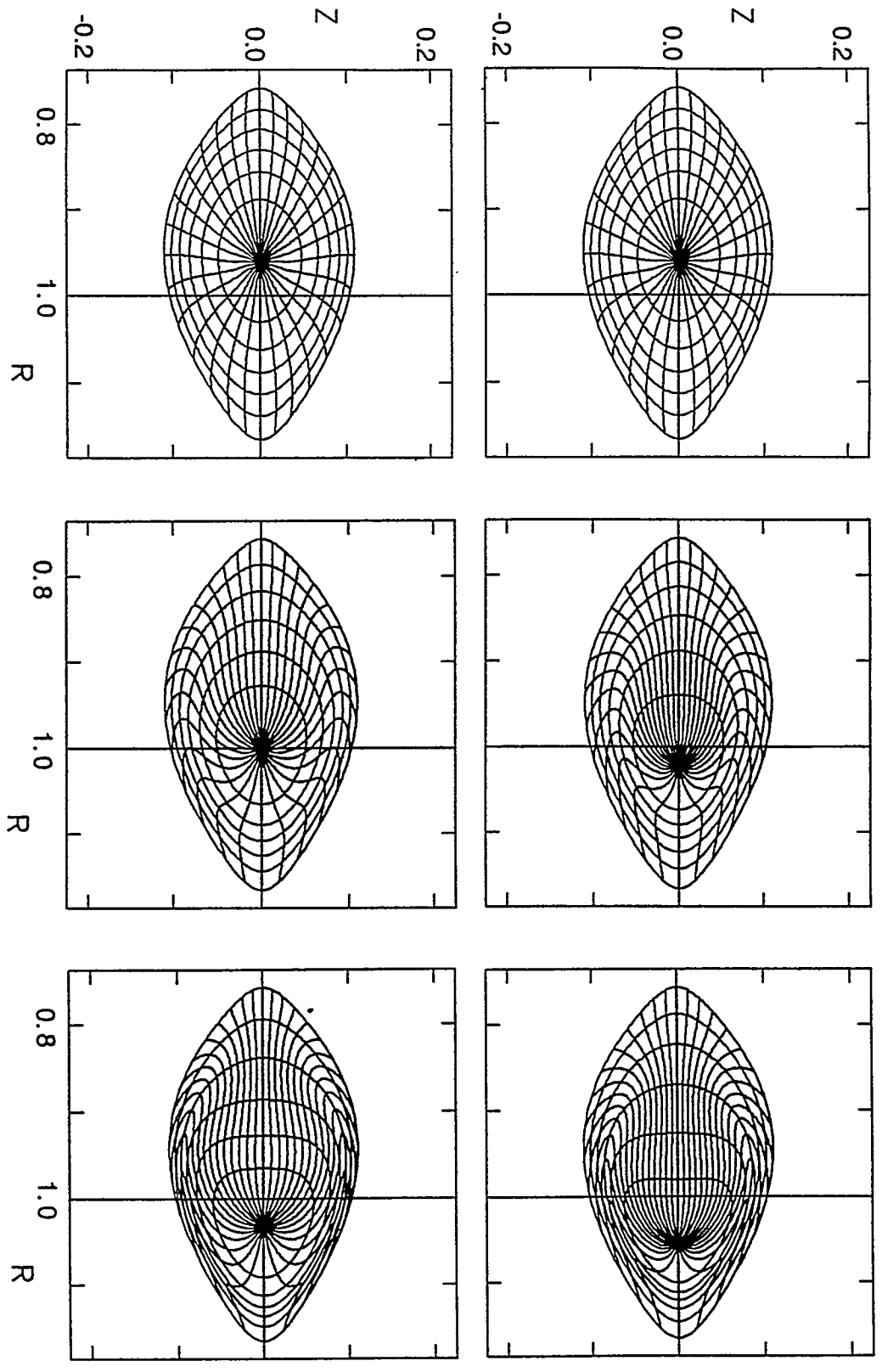

Fig. 2

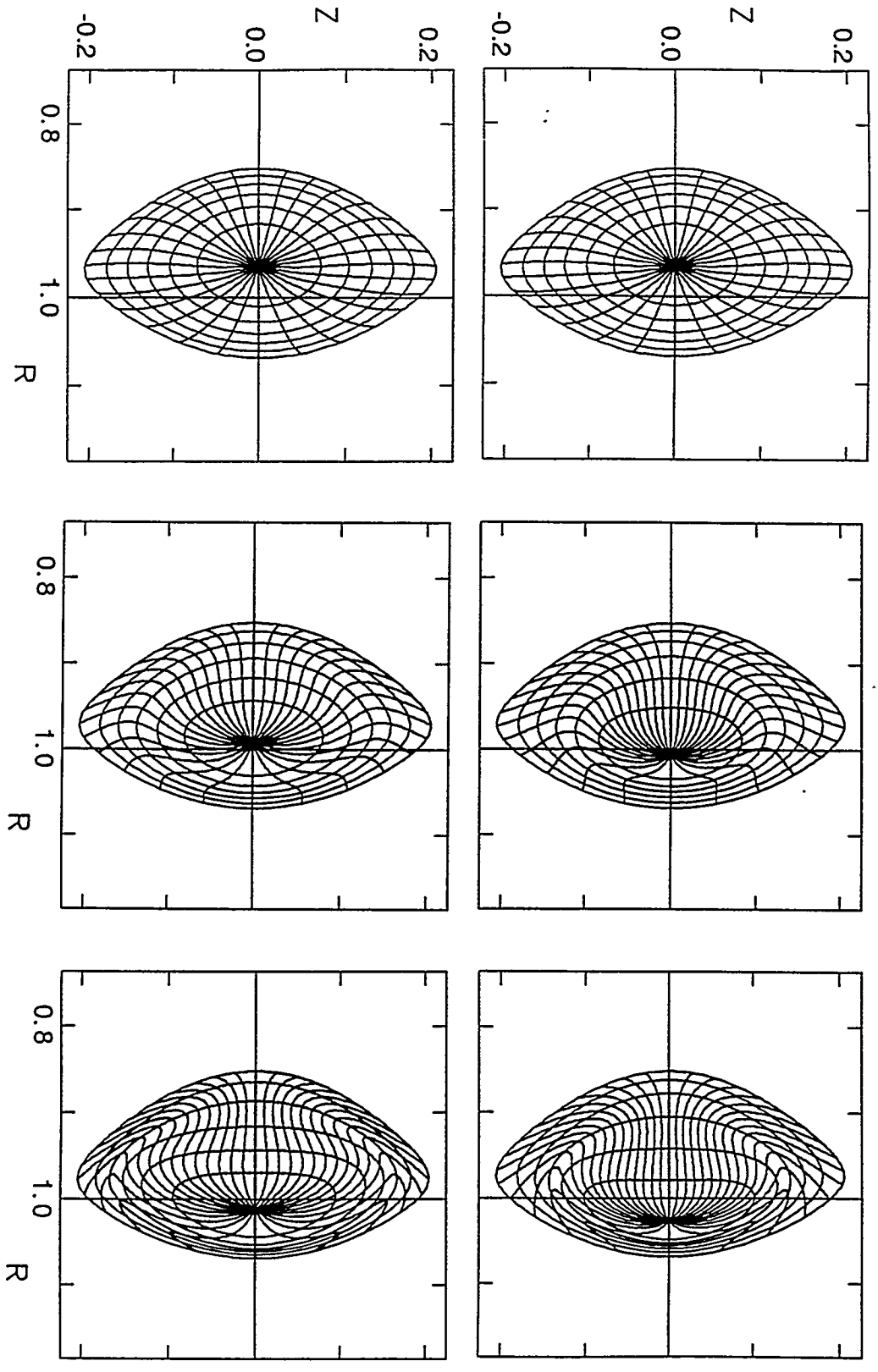

Fig. 3

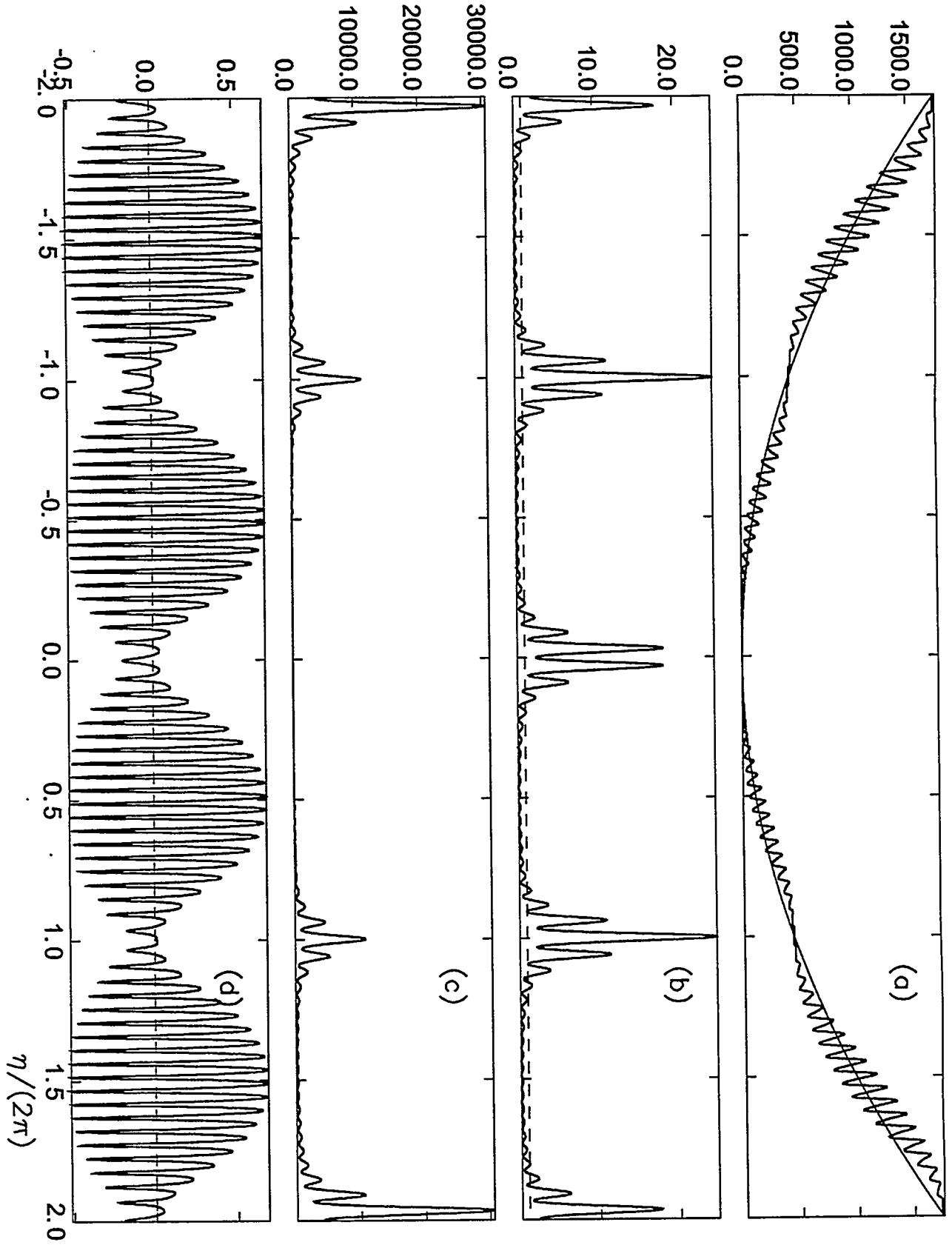
1500.0
1000.0
500.0
0.0
(a)
20.0
10.0
0.0
(b)
30000.0
20000.0
10000.0
0.0
(c)
0.5
0.0
-0.5
(d)
-2.0
-1.5
-1.0
-0.5
0.0
0.5
1.0
1.5
2.0
η/(2π)

Fig. 4

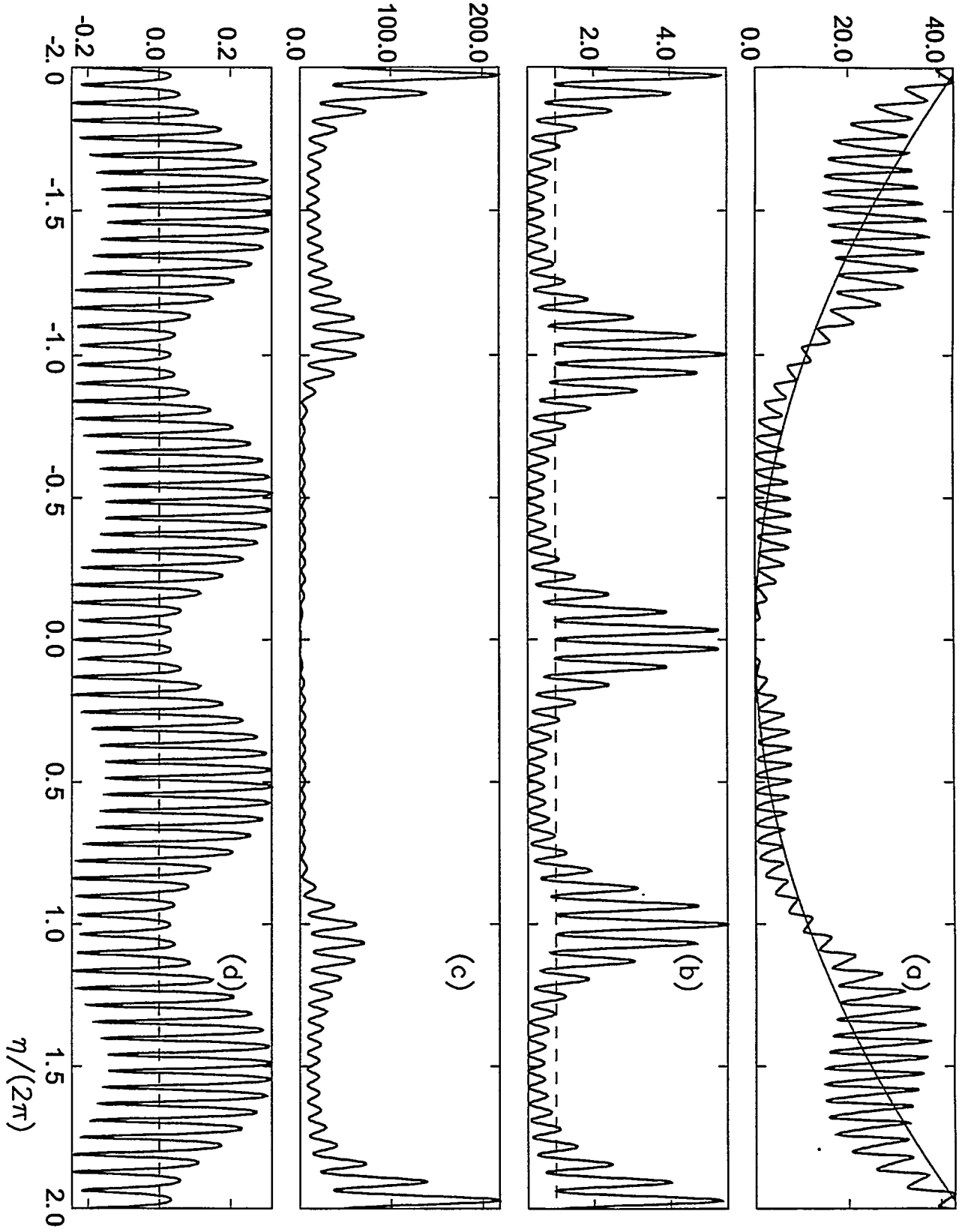
40.0
20.0
0.0
(a)
4.0
2.0
0.0
(b)
200.0
100.0
0.0
(c)
0.2
0.0
-0.2
(d)
-2.0
-1.5
-1.0
-0.5
0.0
0.5
1.0
1.5
2.0
η/(2π)

Fig. 5

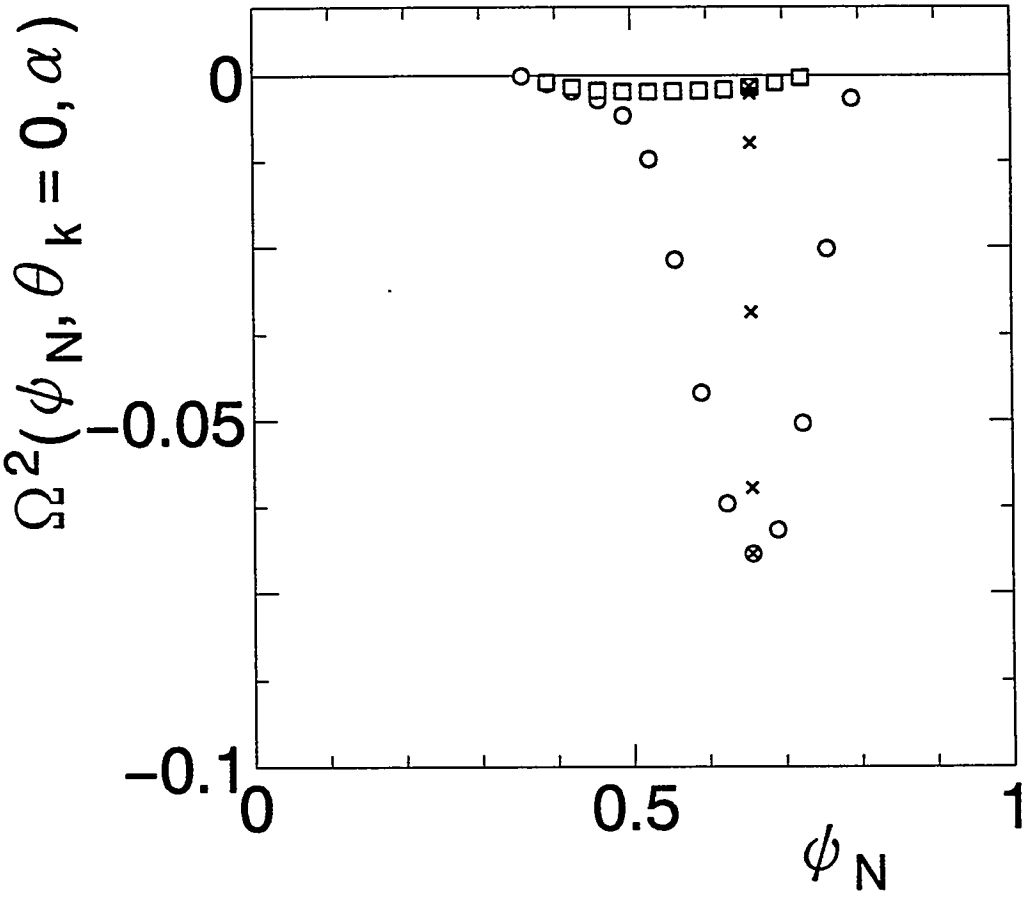

Fig. 6

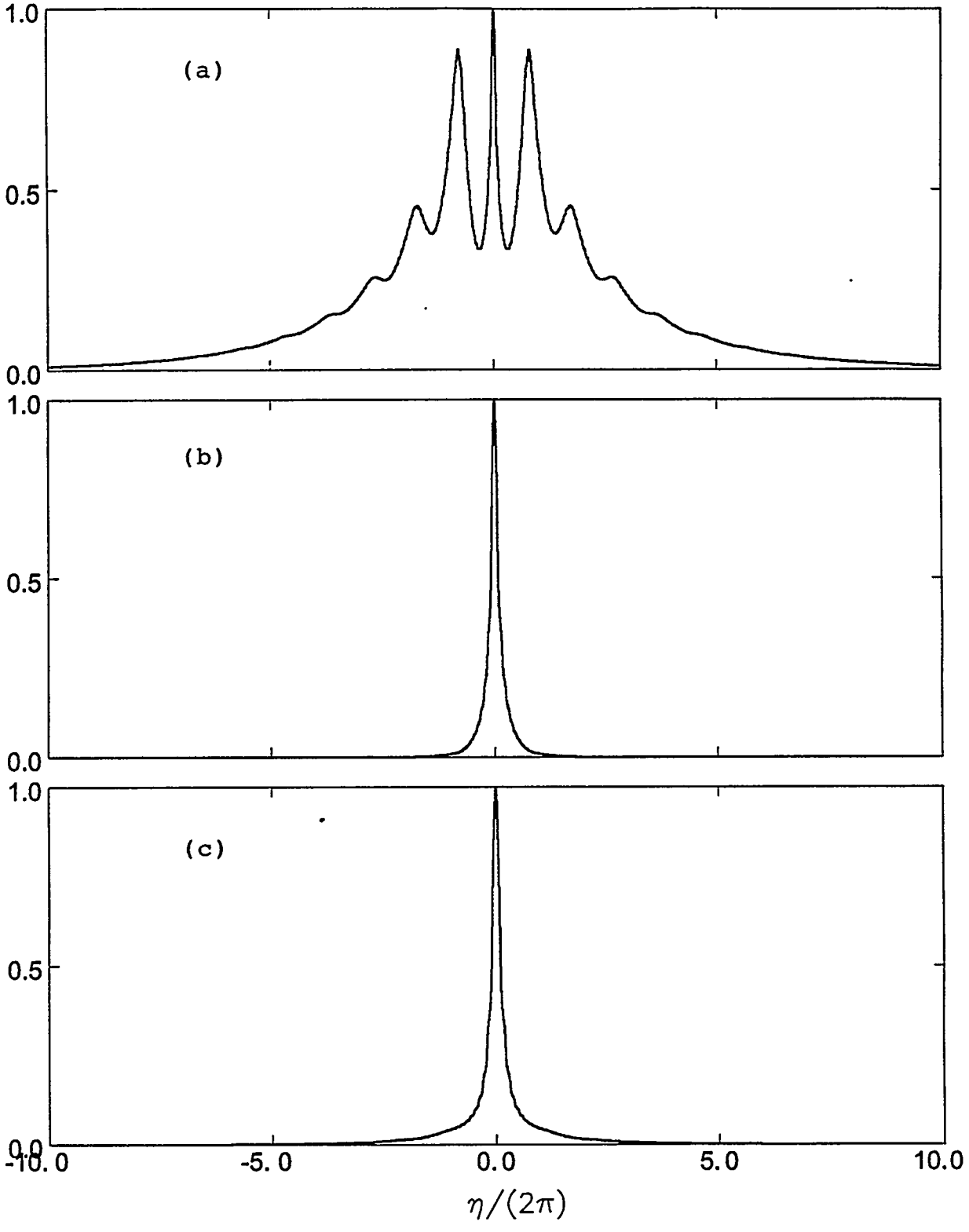

Fig. 7

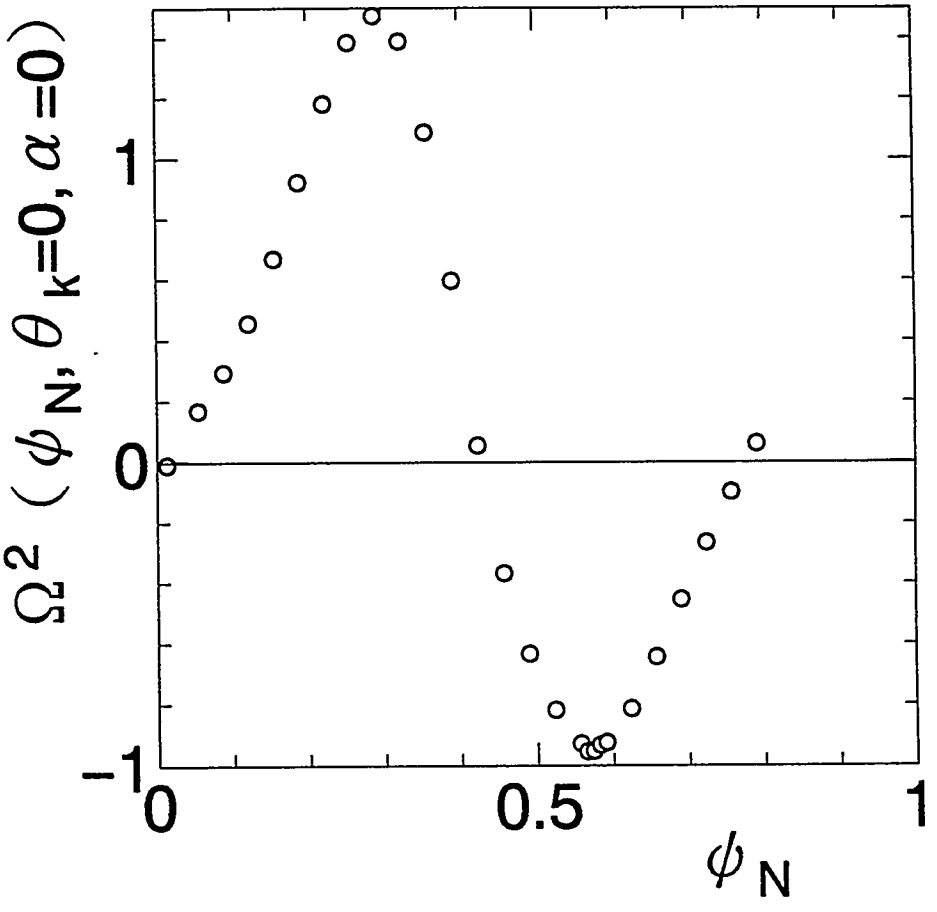

Fig. 8

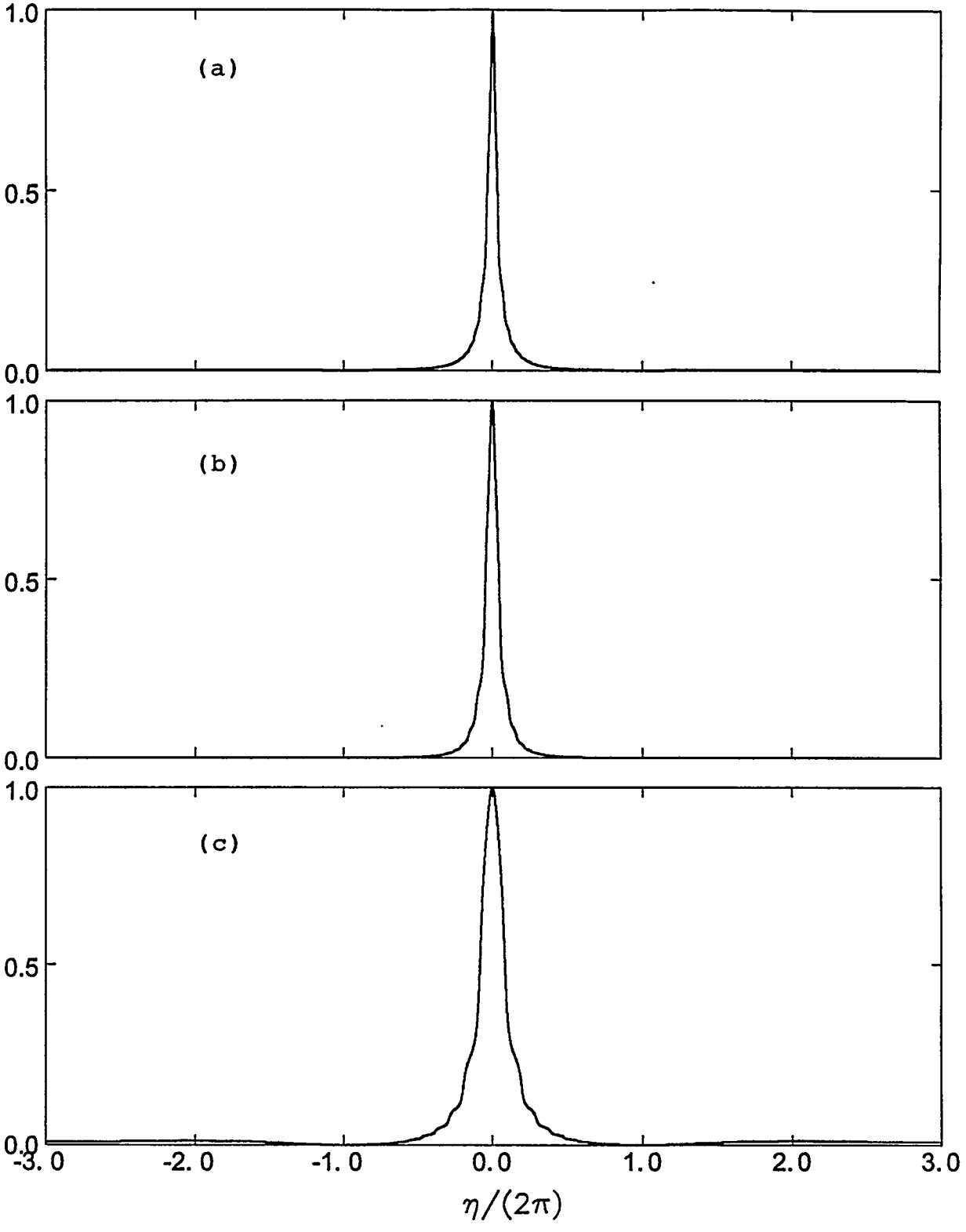

Fig. 9

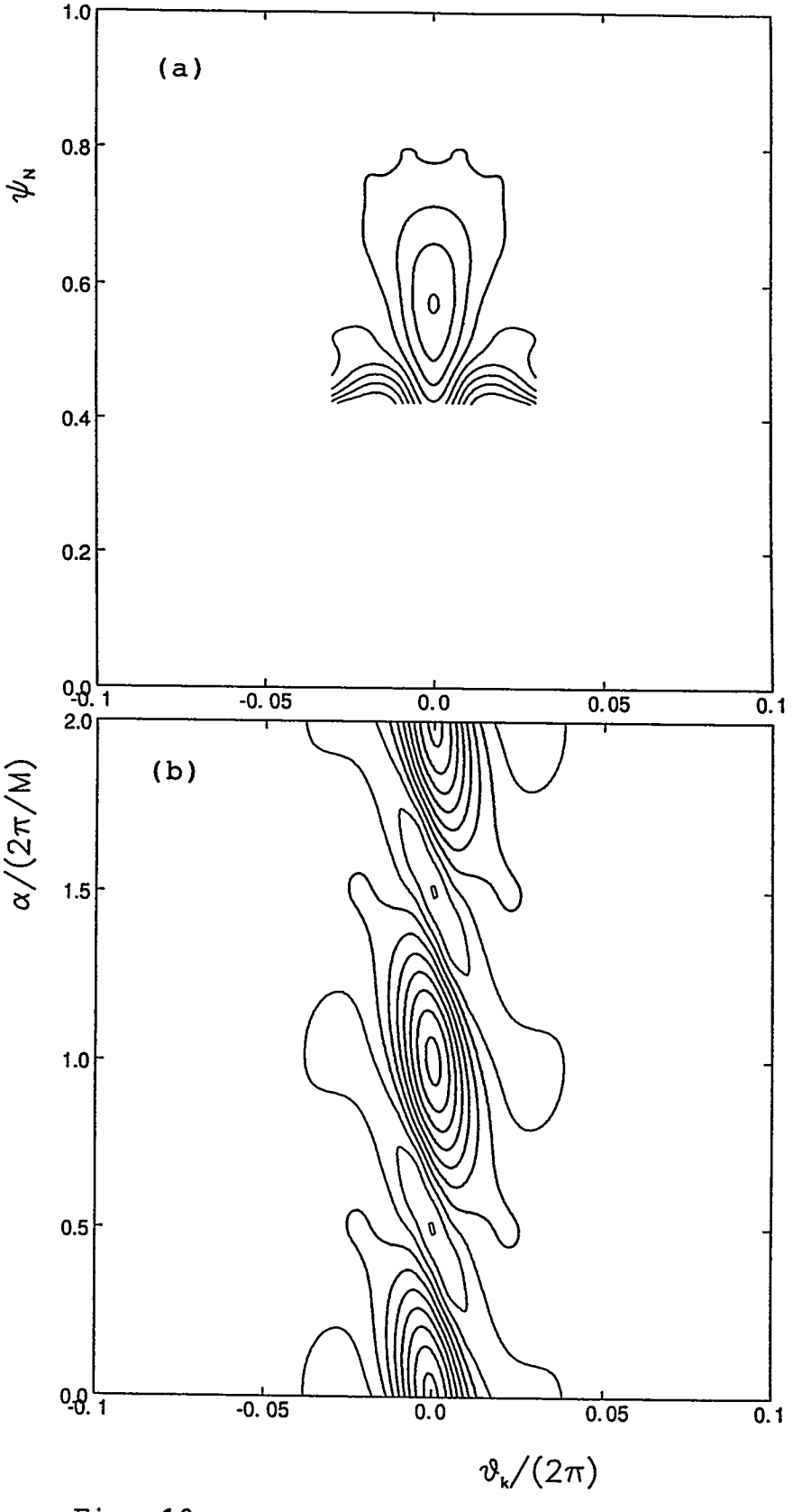
(a)
(b)
ψ_N
$\alpha/(2\pi/M)$
$\vartheta_k/(2\pi)$
1.0
0.8
0.6
0.4
0.2
0.0
2.0
1.5
1.0
0.5
0.0
-0.1
-0.05
0.0
0.05
0.1

Fig. 10

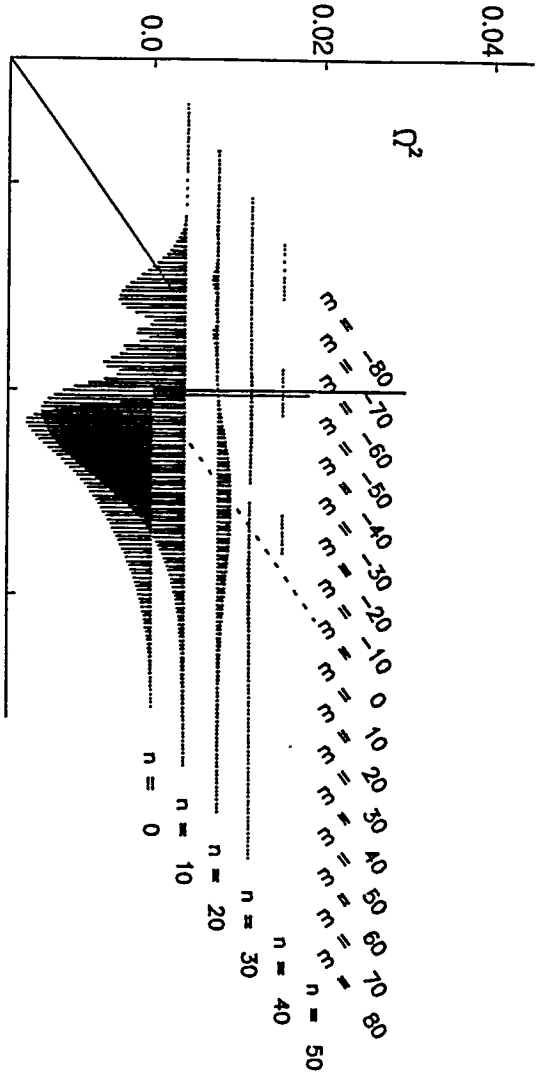
0.0
0.02
0.04
Ω^2
m = -80
m = -70
m = -60
m = -50
m = -40
m = -30
m = -20
m = -10
m = 0
m = 10
m = 20
m = 30
m = 40
m = 50
m = 60
m = 70
m = 80
n = 0
n = 10
n = 20
n = 30
n = 40
n = 50

Fig. 11